JOURNAL OF GEOPHYSICAL RESEARCH, VOL. 113, D14S14, doi:10.1029/2007JD009658, 2008

Aerosol light scattering effect on terrestrial plant productivity and energy fluxes over the eastern United States

Toshihisa Matsui,[1,2] Adriana Beltrán-Przekurat,[3] Dev Niyogi,[4] Roger A. Pielke Sr.,[3] and Michael Coughenour[5]

Received 29 November 2007; revised 21 April 2008; accepted 11 June 2008; published 22 July 2008.

[1] This study reports the first regional-scale assessment of aerosol effects on plant productivity and surface energy fluxes over the eastern United States. Analysis is conducted using an established modeling framework, which is composed of a regional land surface model, regional daily aerosol optical depth (AOD) estimates, and meteorological forcings. The sensitivity experiments were conducted from May to September in 2000 and 2001 over the eastern United States with and without the aerosol light scattering effect. Results show that the aerosol light scattering effect results in enhanced productivity for high-LAI and optimum temperature environments under cloudless-sky conditions around noon, while it results in least productive for low-LAI, low-temperature environments under cloud-sky conditions in early morning or late afternoon. As a result, domain-averaged plant productivities, measured as net primarily production, are changed by -0.71 g C m^{-2} (-0.09%) in 2000 and +5.00 g C m^{-2} (+0.5%) in 2001. These responses of plant productivity and photosynthesis to the aerosol light scattering effect uniquely modulate the surface flux as follows. The aerosol light scattering effect reduces the surface downwelling solar radiation (14.9 W m^{-2} in 2000 and 16.0 W m^{-2} in 2001) and net radiation in vegetation canopy, but simultaneously increases the photosynthesis and stomatal conductance. Consequently, surface latent heat flux (transpiration and evaporation) is reduced by a small amount particularly over the forests, while aerosol loading often results in larger reduction in the sensible heat flux. For the whole domain, latent heat flux is changed by -3.10 W m^{-2} (-2.1%) in 2000 and -3.12 W m^{-2} (-2.1%) in 2001, sensible heat flux is changed by -7.57 W m^{-2} (-12.9%) in 2000 and -8.36 W m^{-2} (-11.3%) in 2001, and surface skin temperature is changed by -0.25 K (-0.1%) in 2000 and -0.27 K (-0.1%) in 2001.

Citation: Matsui, T., A. Beltrán-Przekurat, D. Niyogi, R. A. Pielke Sr., and M. Coughenour (2008), Aerosol light scattering effect on terrestrial plant productivity and energy fluxes over the eastern United States, *J. Geophys. Res.*, *113*, D14S14, doi:10.1029/2007JD009658.

1. Introduction

[2] Diffuse solar radiation is suggested to be more advantageous for plant productivity than direct radiation [e.g., *Goudriaan*, 1977; *Gu et al.*, 2002; *Law et al.*, 2002; *Niyogi et al.*, 2004; *Rocha et al.*, 2004; *Min*, 2005]. This is because diffuse solar radiation is absorbed on the plant canopy more homogeneously than direct radiation, and is efficiently utilized in the photosynthesis process without exceeding the plant photosynthesis capacity. Direct solar radiation is absorbed by the sunlit canopy and usually exceeds the plant photosynthesis capacity when solar elevation is high [*Goudriaan*, 1977; *Gu et al.*, 2002].

[3] Recently the impact of aerosol light scattering on terrestrial plant productivity and carbon sink has been addressed [*Roderick et al.*, 2001; *Cohan et al.*, 2002; *Gu et al.*, 2003; *Niyogi et al.*, 2004; *Chang*, 2004; *Misson et al.*, 2005; *Kanniah et al.*, 2006; *Oliveira et al.*, 2007]. Following the massive eruption of Mt. Pinatubo in 1991, abnormal carbon sinks were observed on the global scale the following year. *Roderick et al.* [2001] and *Gu et al.* [2003] proposed that the volcano eruption-derived sulphate aerosols in the upper troposphere enhanced solar radiation scattering that ultimately increased the terrestrial carbon sink by increasing plant productivity.

[4] *Niyogi et al.* [2004] and *Chang* [2004] provided the first observational evidence of links between variability of routine aerosol optical depths (AODs), diffuse solar

[1]Goddard Earth Sciences and Technology Center, University of Maryland, Baltimore County, Baltimore, Maryland, USA.
[2]NASA Goddard Space Flight Center, Greenbelt, Maryland, USA.
[3]Department of Atmospheric and Oceanic Sciences, Cooperative Institute for Research in Environmental Sciences, University of Colorado, Boulder, Colorado, USA.
[4]Department of Agronomy and Department of Earth and Atmospheric Sciences, Purdue University, West Lafayette, Indiana, USA.
[5]Natural Resource and Environmental Laboratory, Colorado State University, Fort Collins, Colorado, USA.

0148-0227/08/2007JD009658$09.00

radiation, and terrestrial carbon sink for different landscapes over the United States. The statistical results indicated that high AODs tend to increase the daytime carbon sink for forests and croplands sites under cloudless-sky conditions. *Misson et al.* [2005] also reported that the aerosol-driven diffuse radiation contributed to an abnormal increase in the late afternoon carbon sink at the Blodgett Forest (young ponderosa pine plantation) site. *Oliveira et al.* [2007] investigated the effect of biomass-burning-derived aerosols on the terrestrial carbon sink over the Amazon basin during the dry season, and found that plant productivity of forests is enhanced under the moderately thick smoke loading because of an increase of diffuse versus direct solar radiation. *Cohan et al.* [2002] quantitatively analyzed the impact of atmospheric aerosol light scattering on plant productivity using a two-canopy model and idealized sets of environmental parameters, and reported that plant productivity is increased because of moderately thick aerosol loading in cloudless sky.

[5] Several studies, however, have reported a *net* negative impact of aerosols on plant productivity. *Chameides et al.* [1999] reported that the regional aerosols over China, which are often with accompanied with other pollutants, decreased the net surface solar radiation by up to 30%, and could decrease the crop yields. *Mera et al.* [2006] used two crop models to show that a small decrease in radiation level can help increase crop productivity in both C3 and C4 crops (soybean and corn) but a larger decrease in the in coming radiation would ultimately result in reduced yields. Observational analysis by *Niyogi et al.* [2004] and *Chang* [2004] showed that under high aerosol loading and high diffuse radiation conditions, productivity has been increased in croplands and forest sites, in the same study they showed that the carbon sink at both C4 and C3 grass sites is not enhanced for high AODs. *Kanniah et al.* [2006] showed that regional smoke loading tends to depress the carbon sink at a savanna site with a C4 grass understory in northern Australia. These studies agree that high aerosol loadings do not provide advantage for landscape dominated by grasslands.

[6] *Krakauer and Randerson* [2003] investigated tree rings in North America, Europe, and Northern Eurasia, and found that estimated plant productivity in the boreal regions decreased after the eruption of Mt Pinatubo probably because of aerosol-driven temperature feedbacks, as opposed to the hypothesis by *Roderick et al.* [2001] and *Gu et al.* [2003]. *Cohan et al.* [2002] also showed that aerosol loading reduces plant productivity on cloudy sky, and very high aerosol loading can reduce plant productivity even on cloudless sky. *Oliveira et al.* [2007] results indicated that aerosol optical depth larger than 2.7 tends to reduce the net productivity of the Amazon forest. These previous studies indicated that the impact of aerosol light scattering on plant productivity varies depending on the amount of aerosol loading, canopy structure, and environmental conditions.

[7] At present, the impact of aerosol light scattering effects have been tested by statistical analysis using local surface eddy covariance observations [*Gu et al.*, 2002, 2003; *Niyogi et al.*, 2004; *Chang*, 2004; *Misson et al.*, 2005; *Kanniah et al.*, 2006; *Oliveira et al.*, 2007], tree ring observations [*Krakauer and Randerson*, 2003] and by idealized simulations [*Chameides et al.*, 1999; *Cohan et al.*, 2002; *Mera et al.*, 2006]. The next step is to realistically estimate the aerosol light scattering effect on seasonal plant productivity on the regional scale by establishing a regional-scale modeling framework. In addition, it is relatively unclear how aerosol light scattering contributes to changes in surface latent and sensible heat fluxes or radiative temperature [*Chang*, 2004]. Therefore, the impact on aerosol light scattering on surface energy fluxes must be investigated simultaneously, since plant productivity (carbon sink) and surface energy fluxes are tightly coupled by surface water vapor exchange via plant stomata [*Collatz et al.*, 1991].

[8] To that end, this study establishes a realistic regional-scale modeling framework, including (1) a detailed, well-calibrated land surface model with sun-shade canopy considerations and a set of surface boundary conditions and (2) meteorological forcings and aerosol loading to drive the land surface model. Then, model experiments using an offline land surface model with and without aerosol loading are conducted to investigate the aerosol light scattering effect over the eastern United States, where *Niyogi et al.* [2004] and *Chang* [2004] found robust statistical relationships of the aerosol light scattering effect on the plant photosynthesis rate. Indeed, the eastern United States is an ideal region to establish this modeling framework, because of a dense network of local energy and carbon fluxes and aerosol radiation monitoring in different landscapes [*Hicks et al.*, 1996; *Baldocchi et al.*, 2001].

[9] This paper is organized as follows. Section 2 describes the modeling framework and validation and how the meteorological forcings for the experiments were constructed. Section 3 shows the result of the sensitivity experiment using an offline land surface model over the eastern United States. Section 4 discusses the results with respect to previous studies, and summarizes the understanding of aerosol impacts on land surface processes with different landscapes and environmental factors.

2. Regional Modeling Framework

2.1. Land Surface Model

[10] This study uses the Colorado State University (CSU) Unified Land Model (ULM) [*Matsui*, 2007; *Matsui et al.*, 2007] as integrated within the NASA Land Information System (LIS) [*Kumar et al.*, 2006]. CSU ULM includes a ten-layer soil and up to 13 subgrid tiles. The canopy energy budget and photosynthesis are separately diagnosed for sunlit and shade canopies at every model time step, on the basis of the scaled photosynthesis capacity, leaf area index (LAI), and direct and diffuse radiation [*de Pury and Farquhar*, 1997; *Wang and Leuning*, 1998; *Dai et al.*, 2004] (see details in Appendix A). This scaled sun-shade canopy scheme is essentially a big-leaf (one-layer canopy) scheme, but it scales sunlit and shaded components of radiation and canopy photosynthesis properties much more efficiently than a multilayer canopy scheme does [*de Pury and Farquhar*, 1997].

[11] A unique feature of CSU ULM is its tuning-oriented structure. Tuning parameters are identified and hardwired to a parameter estimation model, which enables a rapid and robust development of the land surface scheme on the local and regional scales [*Matsui et al.*, 2007; *Matsui*, 2007].

Table 1. A List of the FLUXNET Observation Sites Used in the Study

ID	Site	Species	Land Cover Classes	Latitude, Longitude (deg)
Morg	Morgan Monroe State Forest, Indiana	sugar maple, tulip poplar, sassafras, white oak, black oak, etc.	deciduous broadleaf forests	39.321, −86.413
Umic	University of Michigan Biological Station, Michigan	bigtooth aspen, quaking aspen, eastern white pine, and northern red oak	deciduous broadleaf forests	45.560, −84.714
Gret	Great Mountain Forest, Norfolk, Connecticut	red maple, eastern white pine, and hemlock	mixed forests	41.967, −73.233
Harv	Harvard Forest, Massachusetts, USA	oak, red maple, black birch, white pine, hemlock, white oak, black oak, and hickory	mixed forests	42.536, −72.172
Duke	Duke Forest, Pine, North Carolina	loblolly pine with red maple, sweetgum, and white oak in the understory.	mixed forests	35.978, −79.094
Will	Willow Creek, Wisconsin	white ash, sugar maple, basswood, green ash, and red oak with sugar maple and ironwood saplings, leatherwood, maidenhair, bracken ferns, and blue cohosh in the understory.	mixed forests	45.906, −90.080
Bond	Bondville, Illinois	annual rotation between corn (C4), 2001, and soybeans (C3), 2000	croplands	40.006, −88.292

Hereafter, we briefly discuss the performance of the ULM during the period of May to September 2000 at seven Fluxnet sites: two sites for deciduous broadleaf forest, four sites for mixed forest, and one site for croplands [*Baldocchi et al.*, 2001] (Table 1). The local-scale simulations are forced by the Fluxnet-observed meteorological variables. Diffuse radiation is estimated from the downwelling broadband shortwave radiation as a function of atmospheric transmittance through the empirical relationship derived from the Integrated Surface Irradiance Study (ISIS) data [*Hicks et al.*, 1996] (see Appendix B). The derived empirical relationship can be considered to be unbiased if integrated over long-term periods. Instantaneous estimation of diffuse radiation has large noise due to three-dimensional radiation scattering [e.g., *Gu et al.*, 2002]. Thus, the model results and observations are compared in terms of long-term averaged values in this study. LAI, land cover, and soil types are estimated from the 1-km-grid product [*Miller and White*, 1998; *Myneni et al.*, 2002; *Hansen et al.*, 2000].

[12] Fluxnet-observed and ULM-computed seasonally averaged diurnal cycles (from May to September) of surface CO_2, latent and sensible heat fluxes are plotted in Figure 1. The ULM-predicted daytime diurnal cycles of latent heat and CO_2 fluxes are in very good agreement with those observed from the Fluxnet sites. There are slight discrepancies (up to 4μmol $m^{-2}s^{-1}$) in the nighttime CO_2 flux at the *UMic*, *Gret*, *Duke,* and *Will* sites mainly due to uncertainties in the nocturnal dark respiration rate parameterized in the soil model. ULM accurately predicts the diurnal cycles of latent heat flux; however, it tends to slightly underestimate the sensible heat flux for most of the sites because of the uncertainties in surface aerodynamic resistance [*Matsui*, 2007].

[13] In addition to these fluxes, we computed light use efficiency (*LUE:* defined as CO_2 flux [μmol m^{-2} s^{-1}] per photosynthetically active radiation flux [μmol m^{-2} s^{-1}] (and multiplied by 100) when the cosine of solar zenith angle is greater than 0.5), and compared it as a function of the diffuse radiation fraction (DRF). *LUE* is an important metric for examining the aerosol light scattering effect on plant photosynthesis [*Gu et al.*, 2002; *Niyogi et al.*, 2004]. Fluxnet observations confirmed the theory and observations in previous studies; namely, *LUE* increases in a high diffuse to direct radiation environment (high DRF) [e.g., *Goudriaan*, 1977; *Gu et al.*, 2002; *Law et al.*, 2002; *Rocha et al.*, 2004; *Min*, 2005]. The ULM also predicted a linear increase in LUE as a function of DRF, similar to the Fluxnet observations. Particularly in this study, slopes of LUE as a function of DRF are important for assessing the sensitivity of the aerosol light scattering effect. Although the ULM predicts slightly larger LUE-DRF slopes than those of the Fluxnet observations in *Morg*, *Gret*, *Harv*, and *Duke* sites, the ULM reasonably captures most of the observed fluxes and LUE-DRF slopes. Therefore, the ULM is appropriate to examine the aerosol light scattering effect on the plant photosynthesis over different landscapes over the eastern United States.

2.2. Meteorological Forcings

[14] In this study, the ULM is run at a 0.25° grid spacing from May to September in 2000 and 2001 over the eastern United States, and is driven by the North American Land Data Assimilation System (NLDAS) meteorological forcing at a 15-min model time step [*Cosgrove et al.*, 2003]. The NLDAS meteorological forcings are composed of a radar-gauge-assimilated hourly precipitation data set, satellite-estimated surface downwelling solar radiation, surface air temperature, water vapor mixing ratio, horizontal wind, and surface pressure derived from NCEP Eta Data Assimilation System (EDAS) output fields. The NLDAS shortwave radiation product does not explicitly separate the radiation effect due to aerosol light scattering. Considering the importance of the aerosol light scattering effect in our analysis, we recalculated the surface shortwave radiation for the sensitivity experiments.

[15] First, we use daily satellite-model-assimilated maps of column aerosol optical depth (AOD) from *Matsui et al.* [2004]. Figure 2a shows the AOD averaged from May to September in 2000 and 2001. The highest AODs (~0.32) appear around Lake Erie and Chesapeake Bay, and gradually decrease toward the outside of the domain down to 0.1. Distribution patterns and magnitude of AODs appear to be quite similar in 2000 (domain-averaged value, m = 0.191)

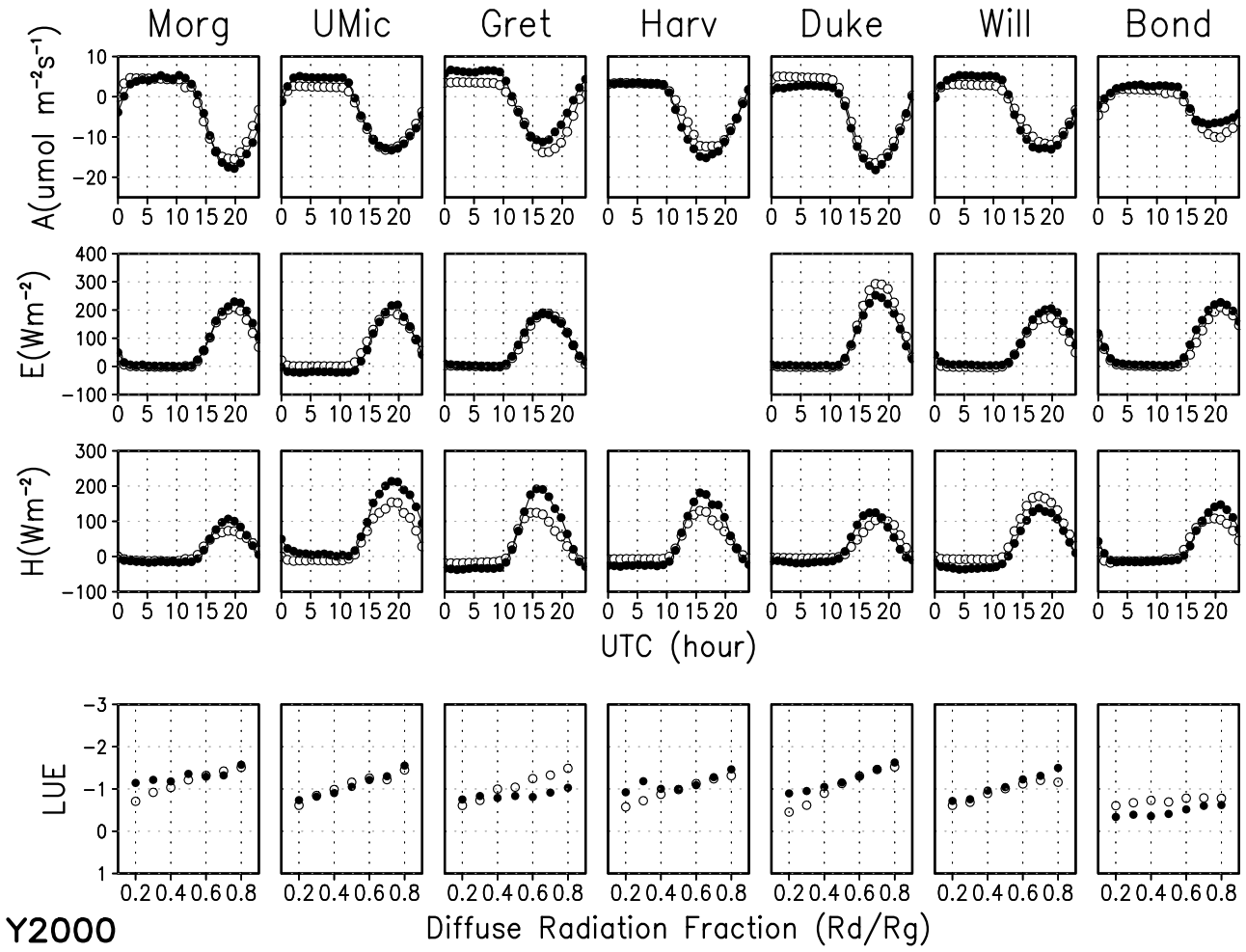

Figure 1. Seasonally averaged diurnal cycles (May–September) of CSU ULM-estimated (open circle) and FLUXNET-observed (solid circle) surface CO_2 flux (A) (μmol m^{-2} s^{-1}), latent heat flux (E) (W m^{-2}), sensible heat flux (H) (W m^{-2}), and light use efficiency (LUE: defined as CO_2 flux (μmol m^{-2} s^{-1}) divided by the photosynthetically active radiation flux (μmol m^{-2} s^{-1}) and multiplied by 100). Note that latent heat flux is not available from the *Harv* site.

and in 2001 (m = 0.190). Detailed discussions and analysis of these AOD maps are given by *Matsui et al.* [2004].

[16] Second, cloud optical properties (liquid water path and optical depth) are estimated from the NLDAS short-wave radiation at every hour (see Appendix C). Figure 2b shows the seasonally averaged daily cloud optical depth (COD). CODs become larger toward the northeastern portion of the domain, and the domain-averaged value is nearly

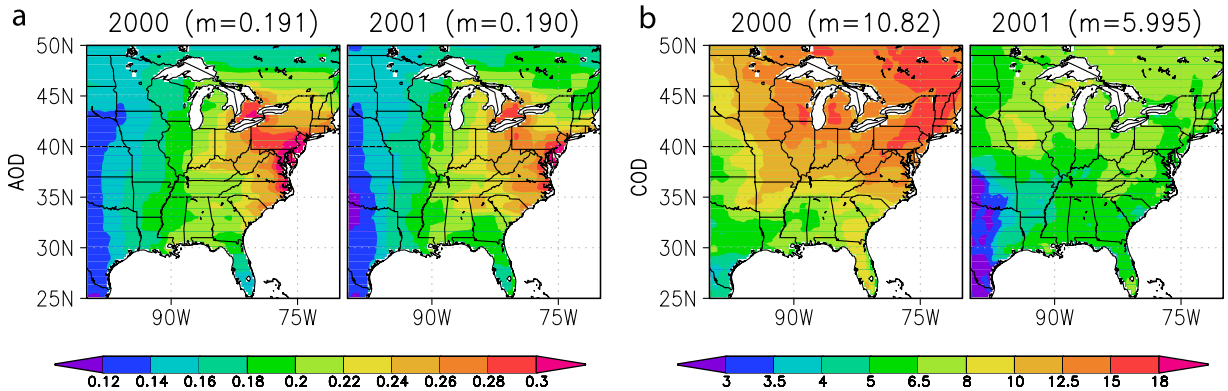

Figure 2. Seasonally averaged (a) MODIS-GOCART assimilated aerosol optical depth AOD (0.55 μm) and (b) NLDAS-derived cloud optical depth (COD). m represents a domain-averaged value. The range, mean, and scatter are also given.

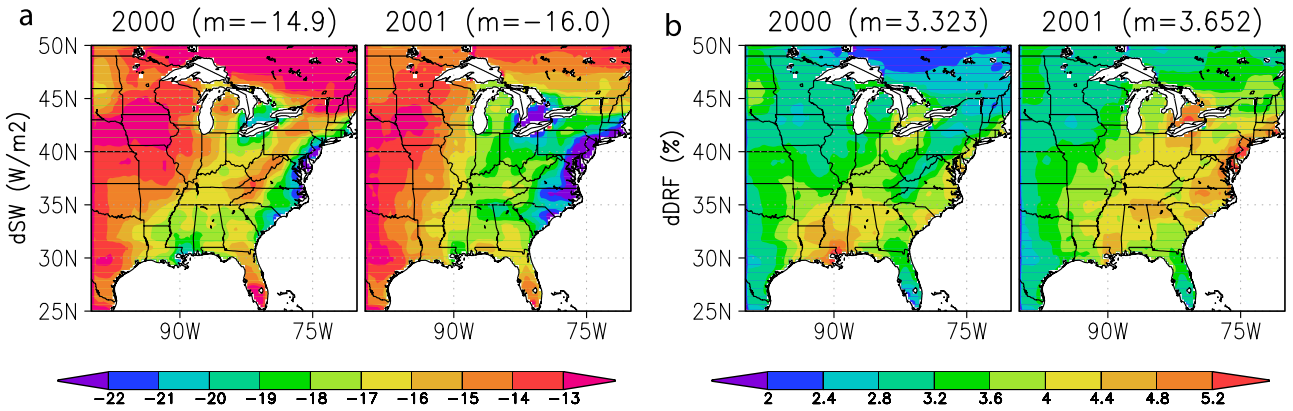

Figure 3. Differences (CTL-POT) in (a) shortwave radiation (dSW) and (b) diffuse radiation fraction (dDRF). *m* represents a domain-averaged value.

twice as high in 2000 (m = 10.82) as in 2001 (m = 5.99). Analysis of the COD variability between 2000 and 2001 is not attempted here. Note that estimated clouds are assumed to be plane parallel (cloud fraction is always unity) in quarter-degree grid boxes. Thus, the effect of highly broken clouds is ignored in this study, although such clouds can create highly diffusive environments [*Min*, 2005].

[17] Using the hourly cloud optical properties, the vertical profiles of pressure, temperature, humidity, and ozone concentrations from sounding climatology for the upper troposphere [*McClatchey et al.*, 1972] and NCEP/NCAR reanalysis for the lower troposphere [*Kalnay et al.*, 1996], downwelling shortwave radiation was computed with and without the satellite-model-assimilated daily AODs by NASA-Langley Fu-Liou radiative transfer model [*Fu and Liou*, 1993; *Charlock et al.*, 2004]. AODs are vertically profiled according to measurements by *Spinhirne et al.* [1980], which confine the aerosol extinction mostly to the boundary layer. Aerosol compositions are estimated from the chemical transport model [*Chin et al.*, 2004], while aerosol optical properties are derived from the Optical Properties of Aerosol and Cloud (OPAC) values [*Hess et al.*, 1998]. The dominant types of aerosol compositions are sulfate and its precursors over the eastern United States [*Malm et al.*, 2004]. Single scattering albedo of these aerosol compositions is nearly unity and effectively enhances downwelling diffuse solar radiation. A seasonally averaged composite of the reconstructed shortwave radiation is compared with the original NLDAS shortwave radiation at each grid point. The result (not shown here) demonstrated that the reconstructed shortwave radiation successfully replicates the NLDAS product within errors of 30 W m^{-2}, while it can separate the radiation effect with and without aerosols. Diffuse and direct radiation components are separated using an empirical relationship (Appendix B).

2.3. Sensitivity Experiments

[18] Using the land surface model (ULM), sensitivity experiments are conducted for shortwave radiation with (a control experiment with the current aerosol loading: CTL) and without aerosol light scattering effect (a potential experiment without the current aerosol loading: POT). Except for the perturbation of downwelling shortwave radiation due to the aerosol light scattering effect, CTL and POT experiments have the identical NLDAS meteorological forcing and boundary conditions (soil texture and vegetation cover). Thus, the difference between CTL and POT can diagnose the aerosol light scattering effect. The simulation periods and study area are consistent with the calibration/validation study [*Matsui*, 2007], which ranges from 1 May to 30 September in 2000 and 2001 over the eastern United States.

[19] Seasonally averaged differences (CTL-POT) in surface downwelling solar radiation (dSW, i.e., the shortwave aerosol direct effect at the surface) ranges from −22 to −13 W m^{-2} (Figure 3a). The domain-averaged differences in dSW are −14.9 W m^{-2} in 2000 and −16 W m^{-2} in 2001. Seasonally averaged differences in diffuse radiation fraction (dDRF) ranges from 2% around the Canadian boreal region in 2000 up to 5% around Lake Erie and Chesapeake Bay in 2001 (Figure 3b). Spatial patterns of dSW and dDRF are clearly correlated, because of the empirical separation of direct and diffuse radiation as a function of atmospheric optical thickness (see Appendix A).

[20] Spatial patterns of dSW and dDRF appear to be correlated with, but slightly different from those of the AODs (see Figures 2 and 3a). These difference are primarily due to the distribution of CODs and the latitudinal trend in solar elevation. For example, AODs in 2000 are relatively larger than those in 2001 over the eastern United States. However, reductions in downwelling shortwave radiation and associated increases in diffuse radiation fractions are relatively larger in 2001. This is because in 2000, cloud cover dominated the region and significantly reduced the incoming solar radiation within the boundary layer. Therefore, the magnitude of the aerosol direct (light scattering) effect is suppressed, since aerosols are mostly concentrated within the boundary layer.

[21] A subgrid land cover map was compiled from the MODIS University of Maryland (UMD) -type 1 km land cover data [*Hansen et al.*, 2000]. The minimum tile fraction was set to 0.13% in the 0.25° grid in order to fully utilize the 1 km information of the MODIS land cover data. Croplands, mixed forest, and deciduous broadleaf forest are the three dominant land cover classes in the study area (Figure 4). Croplands are located mainly in the midwestern United States with some portions close to coastal regions in the southeast. Mixed forests are located in two regions

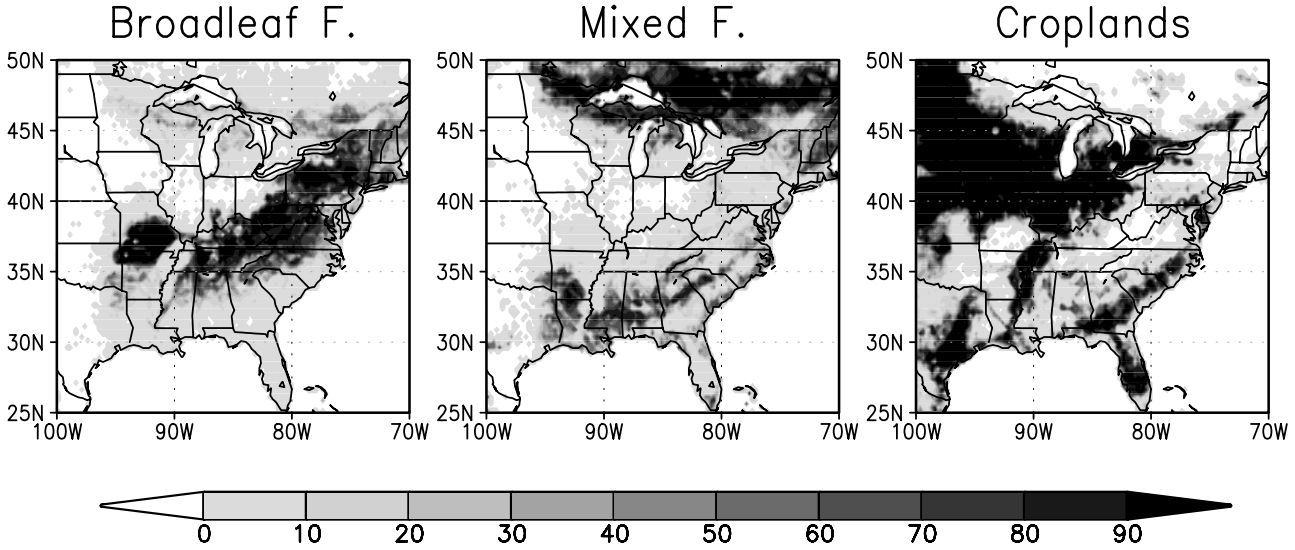

Figure 4. Land cover maps (% of cover within a 0.25° grid box) in the ULM for deciduous broadleaf forest (Broadleaf F.), mixed forest (Mixed F.), and croplands (Croplands).

including the southern United States and Canadian boreal region (at the northern edge of the domain). Broadleaf forests exist in the middle to eastern portions of the domain. Subgrid LAI and stem/dead leaf area index (SAI) are initialized and updated from monthly composites of the 1 km MODIS LAI from Boston University [*Myneni et al.*, 2002]. Details on the surface boundary layer prescription within the ULM are outlined by *Matsui et al.* [2007] and *Matsui* [2007].

3. Results

[22] This section sketches various aspects of the sensitivity experiment results and a detailed discussion is presented in section 4.

[23] Figure 5 shows the spatial map of seasonal (May–September) net primary production ($NPP = \int A_{tot} dt$, where $A_{tot} = A_{sun} + A_{sha}$; A_{tot} is total canopy net photosynthesis; A_{sun} sunlit canopy (direct and diffuse radiation based) net photosynthesis; and A_{sha} is shaded canopy (diffuse radiation based) net photosynthesis) in the CTL experiments and the sensitivity experiments (CTL-POT). The seasonally averaged daily (i.e., integrated over the daytime diurnal cycle) surface latent heat flux (E), sensible heat flux (H), and land surface temperature (LST: skin temperature in this study) are also shown.

[24] The CTL experiment shows that the largest NPP ($\sim$1200 g C m^{-2}) appeared in the deciduous broadleaf and mixed forests in United States, while the smallest NPP is in urban regions, which are scattered in the domain as tiny spots (the first row in Figure 5). NPP is also small in the western edge of the domain. The domain-averaged NPP is 787.0 g C m^{-2} in 2000 and 873.5 g C m^{-2} in 2001. The higher domain-averaged NPP in 2001 is due to less cloudiness in 2001 estimated from the NLDAS radiation (Figure 2b). Sensitivity experiments (CTL-POT) show that aerosol loading increases the NPP up to +35 g C m^{-2} (about 3% increase from the CTL experiment) over forest regions in 2000 and 2001. The value of dNPP in Canadian boreal regions appears to be slightly positive (up to +14 g C m^{-2}) in 2001, but slightly negative (down to −14 g C m^{-2}) in 2000. dNPP appears to be negligible or slightly negative over the croplands and grasslands regions with values as large as −14 g C m^{-2}. The domain-averaged dNPP are −0.71 g C m^{-2} in 2000 and +4.97 g C m^{-2} in 2001, which correspond to about −0.1% and +0.5% change from the CTL experiment, respectively (the first row in Figure 5).

[25] The CTL experiment shows large E (>160 W m^{-2}) over the southern portion of the domain, while smallest E (down to 40 W m^{-2}) exists over the Canadian boreal region, and is loosely coupled with the spatial distribution of seasonal NPP (the second row in Figure 5). The sensitivity experiments show that E is mostly decreased by aerosol loading over croplands and grasslands by as much as −6 W m^{-2}. This is due to the contribution of bare soil evaporation, which represents a high fraction of total evaporation in low-LAI land cover classes, such as grasslands and croplands in the MODIS LAI product [*Myneni et al.*, 2002]. dE is less than 2 W m^{-2} over mixed and deciduous broadleaf forests in the southeastern United States and Canadian boreal region. The domain-averaged dE are slightly negative in 2000 (−3.10 W m^{-2}: −2.1% of the CTL experiment) and in 2001 (−3.12 W m^{-2}; −2.1% of the CTL experiment; the second row in Figure 5).

[26] The CTL experiment shows that H is the highest over the mixed and needleleaf forest in the Canadian boreal region and the southern United States (the third row in Figure 5). The domain-averaged H (58.7 W m^{-2} in 2000 and 73.8 W m^{-2} in 2001) are approximately 50% of E. There are low-H regions in the vicinity of these two highest H regions. The domain-averaged total available energy ($H + E$) is greater in 2001 (218.9 W m^{-2}) than in 2000 (191.5 W m^{-2}) possibly because of less cloudiness in 2001 (Figure 2b). The sensitivity of H to the aerosol loading (dH) is mostly negative over the whole domain with value as large as −12 W m^{-2}, and a domain-averaged dH of −7.57 W m^{-2} (−12.9% of the CTL experiment) in

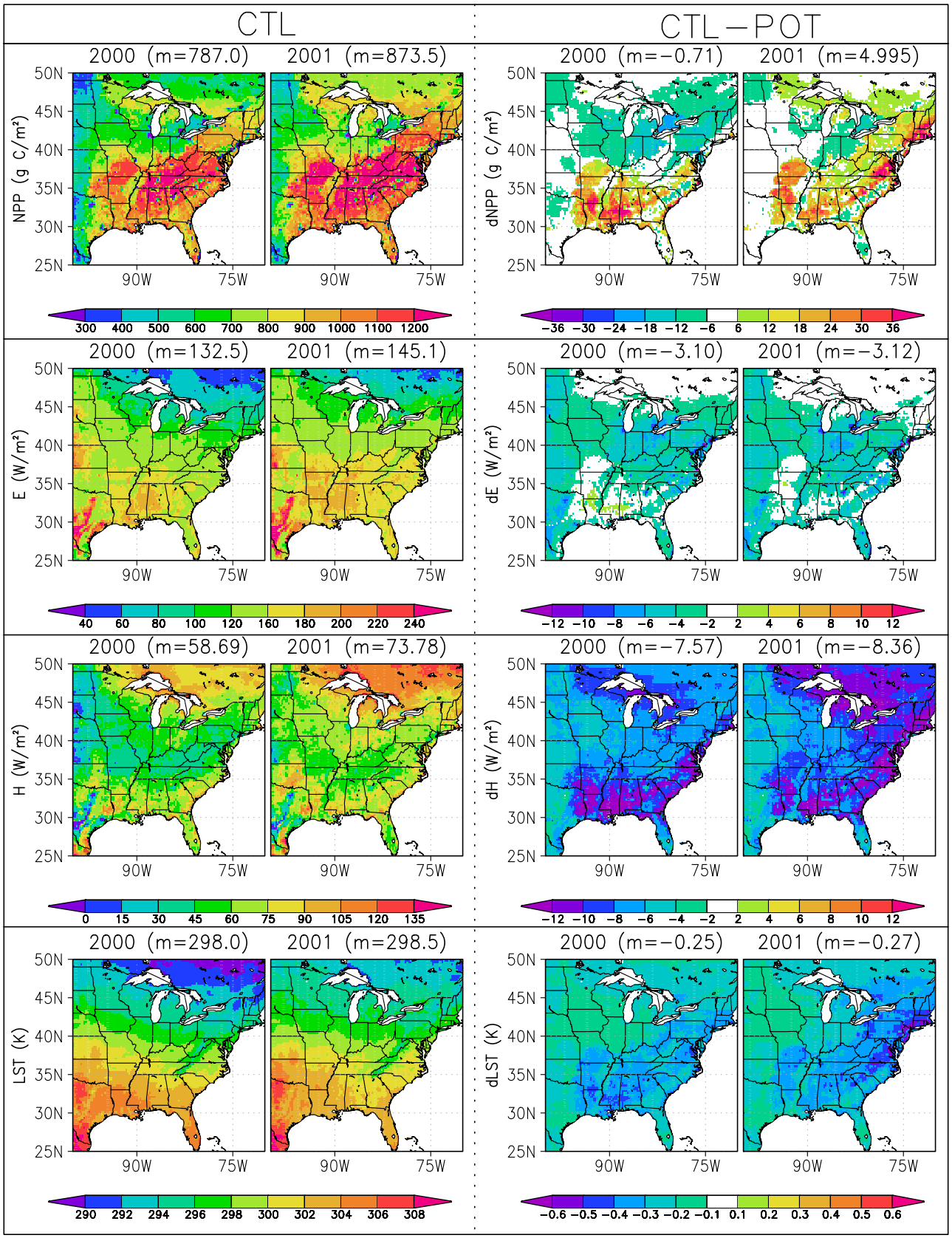

Figure 5. Seasonally averaged control (CTL) and sensitivity (CTL-POT) values of net primary production (NPP), latent heat flux (*E*), sensible heat flux (*H*), and land surface temperature (LST). Note that LST, *H,* and *E* are values integrated over the daytime diurnal cycle. *m* represents a domain-averaged value.

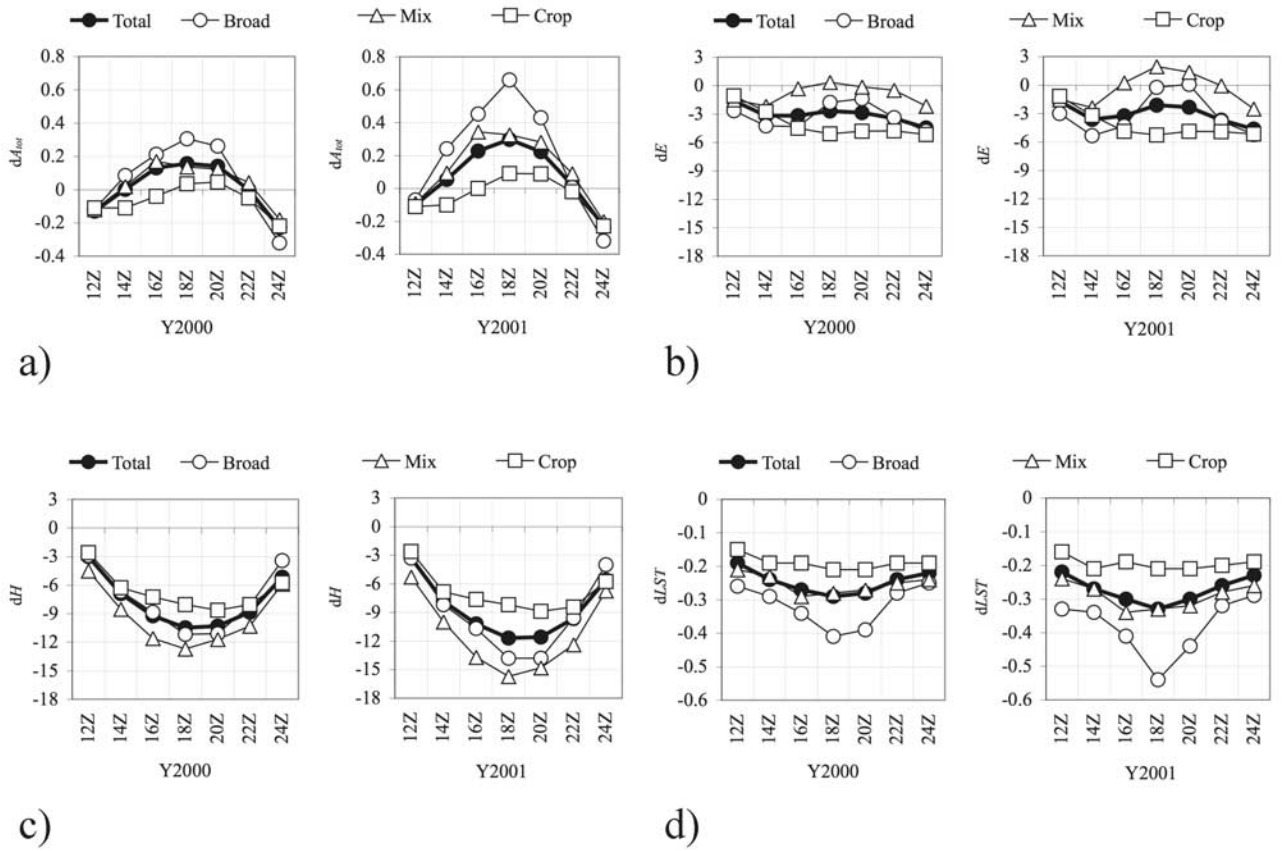

Figure 6. Daytime diurnal cycles of the aerosol light scattering effect on (a) total canopy photosynthesis (dA_{tot}) (μmol m^{-2} s^{-1}), (b) latent heat flux (dE) (W m^{-2}), (c) sensible heat flux (dH) (W m^{-2}), and (d) surface radiative temperature (dLST) (K) to the aerosol loading. Values are averaged over the entire domains, deciduous broadleaf forests (Broad), mixed forests (Mix), and croplands (Crop).

2000 and -8.36 W m^{-2} (-11.3% of the CTL experiment) in 2001, all of which are much greater than those of dE.

[27] The CTL experiment shows that LST peaked in the southwest edge of the domain (up to 308 K), and is decreased toward the northern edge of the domain (down to 290 K) (the fourth row in Figure 5). The northern boreal regions have lower LST in 2000 than in 2001 because of higher cloudiness in 2000 and lower mean solar zenith angle (Figure 2b). Similar to dH, dLST are mostly negative over the entire domain. The lowest value in dLST appears in the East Coast with values as low as -0.5 K.

[28] Figure 6a shows the seasonally averaged daytime diurnal cycles of the sensitivity of total canopy (sunlit plus shaded canopy) net photosynthesis (dA_{tot}) to the aerosol light scattering effect averaged over the entire domain, including the deciduous broadleaf forests, the mixed forests, and the croplands. The diurnal cycles of the domain-averaged dA_{tot} peaked at 1800 UT (+0.16μmol m^{-2} s^{-1} in 2000 and +0.30 μmol m^{-2} s^{-1} in 2001), and have the lowest values in early morning (at 1200 UT) and late afternoon (at 2400 UT). All three land cover classes have similar diurnal cycles; however, their magnitudes are different from each other. The deciduous broadleaf forests have the largest noontime peak values of dA_{tot} (+0.31 μmol m^{-2} s^{-1} in 2000 and +0.66 μmol m^{-2} s^{-1} in 2001), and most values of dA_{tot} are positive throughout the daytime. Croplands have the smallest noontime peak values of dA_{tot} (+0.05 μmol m^{-2} s^{-1} in 2000 and +0.09 μmol m^{-2} s^{-1} in 2001), and dA_{tot} values are mostly negative throughout the day. There are 1-h differences in the timing of the peak dA_{tot} among the three land cover classes. This is simply explained by the longitudinal locations of these land cover classes; for example, most of the croplands are located in the western portion of the domain, while most of the mixed forests are located in the middle to eastern portion of the domain (Figure 4). Thus, noontime over forest classes are 1 h earlier than in the croplands.

[29] The sensitivity of the surface energy fluxes (dH, dE, and dLST) to the aerosol light scattering effect is simultaneously examined in Figures 6b–6d. Peak reductions in dH are -10.5 W m^{-2} and -11.7 W m^{-2} in 2000 and 2001. Among the three land cover types, mixed forest has the largest reductions in dH (-12.7 W m^{-2} in 2000 and -15.7 W m^{-2} in 2001). The domain-averaged dE is consistently negative with a slight increase around local noon. Particularly in 2001, dE becomes positive around noon in the mixed forest. As seen in Figure 5, the results highlighted that the aerosol light scattering effect tends to reduce sensible heat flux more than latent heat flux. The diurnal cycles of response of LST (dLST) are somewhat similar to those of dH. However, broadleaf forest has the

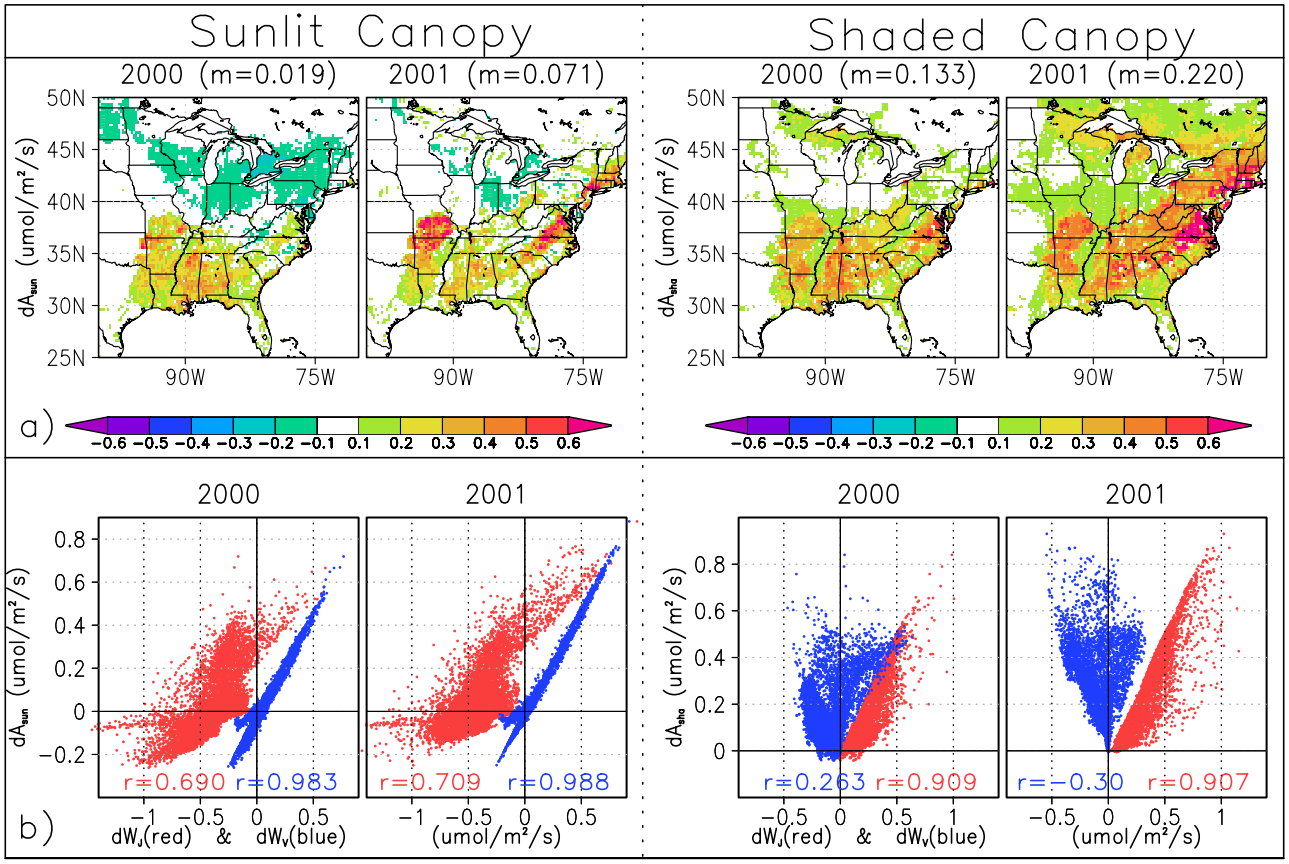

Figure 7. (a) Sensitivity (CTL-POT) of sunlit and shaded canopy photosynthesis (dA_{sun} and dA_{sha}) to the aerosol loading at 1800 UT and (b) scatterplots between each canopy photosynthesis and corresponding light-limited carbon assimilation rate (dW_J) and rubisco-limited carbon assimilated rate (dW_V). Note that W_J and W_V are scaled for sunlit or shaded canopy. m represents a domain-averaged value. r represents a linear correlation coefficient.

largest noontime reduction (−0.41 K in 2000 and −0.54 K in 2001) in d*LST*.

[30] Figure 6 also demonstrates that the aerosol light scattering effect on photosynthesis and surface energy fluxes is most clearly defined around local noon. Thus, we examine the mechanistic responses of sunlit and shaded canopy photosynthesis (dA_{sun} and dA_{sha}) to aerosol light scattering effect at 1800 UT (Figure 7). The sunlit canopy photosynthesis (dA_{sun}) is increased in the southern portion of the domain, while it is decreased in the northern portion especially in 2000. In comparison with dA_{sun} (0.02 μmol m^{-2} s^{-1} in 2000 and 0.07 μmol m^{-2} s^{-1} in 2001 for domain-averaged values), the magnitude of increases in shaded canopy photosynthesis (dA_{sha}) appears to be larger and more extensive over the domain (0.13 μmol m^{-2} s^{-1} in 2000 and 0.22 μmol m^{-2} s^{-1} in 2001 for the domain-averaged values). dA_{sun} is particularly large over the forest regions, which has a higher LAI and large fraction of shaded canopy. Thus, on the basis of our modeling framework, the aerosol light scattering effect enhances the shaded canopy photosynthesis, which leads to increases in the regional net plant productivity over the forest regions as shown in Figures 6a and Figure 5.

[31] Figure 7b investigates the response of the photosynthesis parameterization in more detail. The scatterplots show changes in sunlit and shaded canopy-scaled rubisco-limited carbon assimilation rate (dW_v) and light-limited carbon assimilation rate (dW_J), as linked to changes in sunlit and shaded canopy photosynthesis (dA_{sun} and dA_{sha}). As shown in Table A2 in Appendix A, the light-limited (W_J) and rubisco-limited rates (W_v) are essential factors that control the canopy photosynthesis rate. Generally, an increase in absorbed solar energy in canopy linearly elevates W_J (equation (4) in Table A2 in Appendix A). However, this linear increase of W_J can be impeded by the limitation of the photosynthesis capacity (W_v) (equation (3) in Table A2 in Appendix A). The scatterplots demonstrate that the variability of dA_{sun} at 1800 UT is linearly correlated with the variability of dW_v (r = 0.98 in 2000 and r = 0.99 in 2001), while the dW_J is less correlated with canopy photosynthesis; that is, sunlit canopy photosynthesis is in a rubisco-limited environment around noontime. In contrast, variability of dA_{sha} is strongly correlated with the variability of dW_J (r = 0.91 in 2000 and r = 0.91 in 2001), while the variability of dW_v does not explain the variability of dA_{sh}; that is, the shaded canopy photosynthesis can also be in a light-limited environment around noontime. This is the fundamental basis of how sunlit and shaded canopy photosynthesis responds to the light environment around noon in the sun-shade canopy model used in our modeling

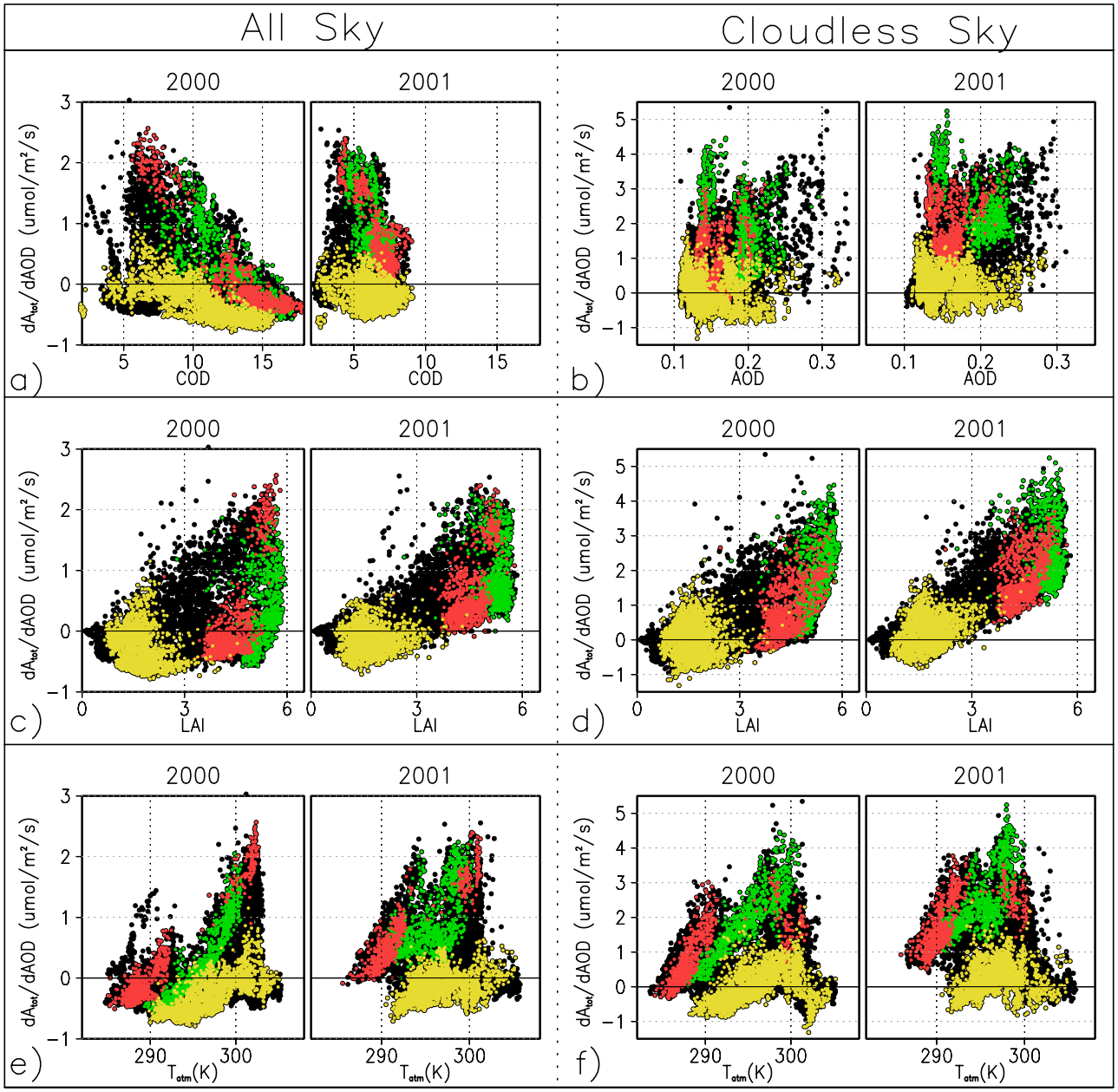

Figure 8. Scatterplots of the seasonally averaged normalized aerosol light scattering effect (defined as dA_{tot}/dAOD) and different factors, including cloud optical depth (COD), aerosol optical depth (AOD), leaf area index (LAI), and 10 m above-canopy air temperature (T_{atm}). All variables are integrated over daytime diurnal cycle. The scatterplots are further clustered for deciduous broadleaf forests (green), mixed forests (red), and croplands (yellow) in all-sky and cloudless-sky conditions. Note that the black dots that are not covered by colored dots are land cover types that are not categorized in the three dominant types.

framework. Although not shown here, both shaded and sunlit canopy photosynthesis becomes a light-limited environment in the early morning or late afternoon; therefore net canopy response to aerosol (and cloud) light scattering effect becomes negative because of reduced net canopy radiation as shown in the diurnal cycle plots (Figure 6a).

[32] As shown in Figures 6 and 7, the solar zenith angle controls the diurnal cycle of the light scattering effect on plant productivity. However, the solar zenith angle does not explain the spatial variability of the aerosol light scattering effect on NPP as seen in the first row of Figure 5 and also does not explain the various degrees of the diurnal cycle of the aerosol light scattering effect averaged over different landscapes depicted in Figure 6a. Therefore, we further analyze the response of the aerosol light scattering effect on plant productivity by linking to other environmental parameters, which were discussed in previous studies [*Cohan et al.*, 2002; *Oliveira et al.*, 2007; *Niyogi et al.*, 2004; *Krakauer and Randerson*, 2003]. For this, we first normalized the aerosol light scattering effect by unit AOD,

Table 2. Linear Correlation Coefficients Between the Normalized Aerosol Light Scattering Effects (dA_{tot}/dAOD) and Different Factors, Corresponding to Figure 8

	All-Sky Conditions					
	COD		LAI		T_{atm}	
Year	2000	2001	2000	2001	2000	2001
Total	−0.43	−0.04	0.49	0.76	0.47	0.06
Broad	−0.77	−0.64	0.24	−0.15	0.91	0.58
Mix	−0.93	−0.82	0.76	0.62	0.94	0.93
Crop	−0.73	−0.25	−0.24	0.05	0.75	0.39
	Cloudless-Sky Conditions					
	AOD		LAI		T_{atm}	
Year	2000	2001	2000	2001	2000	2001
Total	0.38	0.35	0.70	0.83	0.12	0.19
Broad	−0.37	−0.52	0.42	−0.11	0.90	0.69
Mix	0.31	0.18	0.60	0.50	0.70	0.66
Crop	0.11	−0.11	0.03	0.32	0.43	0.22

defined as an increase in total canopy photosynthesis per unit AOD (dA_{tot}/dAOD), since the AOD is heterogeneously distributed in space. Then dA_{tot}/dAOD is linked to the cloud optical depth (COD), aerosol optical depth (AOD), leaf area index (LAI), and 10 m above-canopy atmospheric temperature (T_{atm}). We also made an attempt to review the effect of soil moisture impacts on the aerosol light scattering effect, but the results were variable and hence not included in this discussion. The scatterplots are further clustered for deciduous broadleaf forests, mixed forests, and croplands in all-sky and cloudless-sky conditions. Linear correlation coefficients for all scatterplots in Figure 8 are summarized in Table 2.

[33] First, the effects of COD are shown in all-sky conditions (Figure 8a), since effects of COD on the aerosol light scattering effect were demonstrated by the simulation study by *Cohan et al.* [2002]. Their study indicates that the aerosol light scattering effect on plant productivity become negative under high COD because of large reductions in net incoming solar radiation at the surface. Figure 8a shows that the variability of dA_{tot}/dAOD declined from low COD to high COD, particularly in 2000 ($r = -0.43$). In 2001, the correlation between COD and the normalized aerosol light scattering effect is small (−0.04), because of the low variability of COD (<10). When clustered for different land cover classes, COD effects explain the variability of dA_{tot}/dAOD even better. The COD effects in mixed forests have linear correlations of −0.93 in 2000 and −0.82 in 2001 (Table 2). Two separated clusters of scatterplots in mixed forest represent the mixed forests class in the Canadian boreal regions (for high COD) and in the southern United States (for low COD).

[34] Second, the effects of AOD are examined in cloudless-sky conditions (Figure 8b). *Cohan et al.* [2002] found that the aerosol light scattering effect changes from positive to negative ranging from low AOD and high AOD. *Oliveira et al.* [2007] also shows that net plant productivity is increased under moderately thick smoke loading over the Amazon basin, but AOD larger than 2.7 tends to reduce net plant productivity. Therefore, we expect the positive (negative) normalized aerosol scattering effect under low (high) AOD. However, Figure 8b shows that on a regional scale, there is no clear relationship for the whole domain and each land cover class. The reason for this result is that the distribution of seasonal AOD over the eastern United States is relatively low, up to 0.3. Probably a much larger range of AOD (or shorter temporal scale instead of seasonally averaged value) may yield the nonlinear effect demonstrated by *Cohan et al.* [2002] and *Oliveira et al.* [2007].

[35] The variation of dA_{tot}/dAOD in cloudless-sky conditions is nearly twice as high (up to 5 μmol m^{-2} s^{-1} per unit AOD) as that for cloudy-sky conditions (up to 2.5μmol m^{-2} s^{-1} per unit AOD) in Figures 8a and 8b (note that Figures 8a and 8b use different scales in the y axis). In addition, as indicated by the strong diurnal cycles of the aerosol light scattering effect on photosynthesis in Figure 6a, if it is averaged only at 1800 UT (around local noon) for a season, dA_{tot}/dAOD becomes even larger (up to 10 μmol m^{-2} s^{-1} per unit AOD; not shown here). This value is quantitatively close to the local observational statistics, which focused on cloudless-sky conditions during high solar elevation over the eastern United States [*Niyogi et al.*, 2004; *Chang*, 2004].

[36] Third, the effects of LAI changes are examined in all-sky conditions (Figure 8c) since the variability of LAI should be important to determine the amount of shaded canopy LAI and canopy structure [*Niyogi et al.*, 2004]. Scatterplots show the apparent positive correlation between LAI and dA_{tot}/dAOD for the entire domain in 2000 and 2001. The correlation is stronger in cloudless-sky conditions ($r = 0.70$ in 2000 and $r = 0.83$ in 2001) (Figure 8d) than those in all-sky conditions ($r = 0.49$ in 2000 and $r = 0.76$ in 2001), because the strong COD effect impedes these correlations in all-sky conditions. This relationship clearly suggest why the aerosol light scattering effect on the seasonal NPP (the first row of Figure 5) and the diurnal cycle of photosynthesis (Figure 6a) is largely positive over the forest regions characterized with larger (>3) LAI in the MODIS LAI product [*Myneni et al.*, 2002]. Unlike the entire domain, LAI does not explain the variability of dA_{tot}/dAOD for the individual land cover class (Table 2). This is mainly because the variability of LAI is small within the same land cover class. Therefore this result supports the idea that variability of the aerosol light scattering effect between different landscapes is due to different canopy structure and LAI [*Niyogi et al.*, 2004].

[37] Finally, the effects of T_{atm} are examined in all-sky and cloudless-sky conditions (Figures 8e and 8f). The temperature effect on the aerosol light scattering effect was hypothesized by *Krakauer and Randerson* [2003]. They hypothesized that the aerosol light scattering effect on plant productivity could be negative over cold regions because of the reduction in the surface temperature and thus the photosynthesis kinetic function. Figure 8 shows that the scatterplots appear to be triangular-shaped and clustered. For the individual land cover class, the correlations are very high especially for all-sky conditions in 2000 (up to 0.94 for mixed forests). Correlations become slightly lower than all-sky conditions in 2000 for the rest of the cases, in particular with cloudless-sky conditions. This is due to a combination of positive and negative temperature feedbacks, and can be clearly seen in the scatterplots of croplands in cloudless-sky conditions in 2000. In the range of T_{atm} from 290 K to 300 K, dA_{tot}/dAOD increases for higher T_{atm}. However, for T_{atm} higher than ~300 K, additional increases in T_{atm} tend

to decrease $dA_{tot}/dAOD$. This relationship closely mimics the kinetic function in photosynthetic capacity (equation (A3) in Appendix A). The scatterplots suggest that the aerosol light scattering effect becomes small or negative in the cold-temperature environment, and thus supports the hypothesis of *Krakauer and Randerson* [2003].

4. Discussion

[38] The sensitivity experiments (CTL-POT) showed that the aerosol light scattering effect increases NPP over forest regions in the eastern United States, while it has a negative or negligible impact on the NPP over crop regions (Figure 5). Aerosol loading regionally increases plant productivity mostly around noontime, while there is a smaller or negative impact in the early morning and late afternoon (Figure 6a). This is due to sunlit canopy photosynthesis in a light-saturated (light-limited) environment around noontime (in the early morning or late afternoon), while shaded canopy photosynthesis is always in a light-limited environment (Figure 7). Thus, aerosol-driven increases in diffuse radiation and simultaneous decrease in direct radiation effectively increase total canopy photosynthesis.

[39] The regional variability of the aerosol light scattering effect is explained well by the LAI characteristics in different land cover types; that is, the land cover types with high LAI (such as forests) tend to have a large portion of shaded canopy, while the ones with low LAI (such as croplands and grasslands typically in the MODIS LAI product [*Myneni et al.*, 2002]) have less shaded canopy (Figure 8d). Since the enhancement of the diffuse radiation based shaded canopy photosynthesis is the essential mechanism (Figure 7), the aerosol light scattering effect became productive (unproductive) for high-LAI (low-LAI) regions (Figure 5). This result, the increase in NPP over the forests, is consistent with the studies of *Gu et al.* [2002], *Niyogi et al.* [2004], *Misson et al.* [2005], and *Oliveira et al.* [2007]. All of these studies reported the positive aerosol light scattering effect on plant productivity. This results in a decrease in NPP over the grasslands and is consistent with the studies of *Niyogi et al.* [2004], and *Kanniah et al.* [2006].

[40] Croplands tend to have low LAI in the MODIS product, which have a small (high) fraction of shaded (sunlit) canopy. Thus, a response of shaded canopy photosynthesis essentially does not affect the total canopy photosynthesis, and the sunlit canopy photosynthesis dominates the total canopy photosynthesis. Thus, croplands are more susceptible to aerosol-cloud-driven reduction in direct radiation (Figure 8a). However, low LAI in the croplands could be an artifact of the MODIS LAI product [*Myneni et al.*, 2002]. The typical footprint sizes of the MODIS visible channels are $\sim$1 km, which may not resolve the subgrid fraction (clumping) of LAI in croplands. If the clumping effect is properly accounted for, LAI values and simulation results would be altered to some degree. In fact, the observational study by *Niyogi et al.* [2004] shows the clear positive correlation between AOD and photosynthesis rate in the cropland Fluxnet sites.

[41] For the individual land cover class, the spatial variability of seasonal cloud optical depth (COD) appears to be a critical factor that controls the aerosol light scattering effect on plant productivity (Figure 8). These relationships mostly explain the coherence between the spatial variability of dNPP (the first row of Figure 5) and COD (Figure 2b). The high COD in 2001 over the northern portion of the domain reduces the aerosol light scattering effect on NPP with values of -14 g C m^{-2} over the Canadian boreal forest, in comparison with the positive dNPP in 2001. This result is consistent with the idealized simulation study by *Cohan et al.* [2002]; for example, NPP is increased by aerosol loading on cloudless-sky days, while it is decreased on cloudy days because of the large reduction of solar irradiance on the canopy. This is because sunlit canopy photosynthesis is in a light-saturated (light-limited) environment in cloudless (cloudy) sky. In general high-latitude areas such as Boreal regions are frequently overcast [*Rossow and Schiffer*, 1991], thus the aerosol light scattering effect is expected to be minimal or even negative in those regions. This could be one of the reasons that explains why the tree ring-estimated NPP over the Arctic and tundra regions decreased after the eruption of Mt. Pinatubo [*Krakauer and Randerson*, 2003].

[42] It is also known that aerosols can modulate the cloud microphysics and cloud structures [e.g., *Matsui et al.*, 2004, 2006; *Lin et al.*, 2006; *Tao et al.*, 2007]. Yet, this aerosol indirect effect was not used in this study because of high levels of model input uncertainty. However, it can be speculated that the aerosol light scattering effect (mostly productive in the cloudless sky) can be canceled by the significant reduction in surface irradiance, if high concentrations of aerosols simultaneously increase cloudiness.

[43] In addition to the COD, the spatial variability of seasonally averaged 10 m above-canopy atmospheric temperature (T_{atm}) also helps explains the variability of the normalized aerosol scattering effect on NPP ($dA_{tot}/dAOD$) for the individual land cover class, particularly in the cloudless sky (Figure 8f). Canopy temperature controls light-saturated, i.e., Rubisco-limited, photosynthesis rate via equations (A2a, A2b) and (A3) in ULM (Appendix A). The normalized aerosol light scattering effect on NPP peaks at the optimum temperature around at 300 K, and it becomes lower toward the colder or hotter temperature. Thus, the low temperature in the northern portion of the domain, such as the Canadian boreal regions, created a sunlit-canopy-photosynthesis environment susceptible to a reduction in near-surface temperature. This result is close to the hypothesis put forth by *Krakauer and Randerson* [2003]. Their detailed analysis shows that the tree ring-estimated NPP were slightly increased in temperate forests (30–45°N) and decreased in boreal forests (45–60°N and >60°N) after the eruption of Mt. Pinatubo. They speculated that the low-temperature environment regulates the reduction of NPP in boreal forest.

[44] In the simulation domain, mixed forests are located in the southern United States and Canadian boreal regions (Figure 4). The optimum temperature (T_{opt}) for photosynthesis capacity (equation (A3) in Appendix A) has been set at 307 K for the mixed forests, which correspond to the seasonally averaged daily LST in the southern United States (Figure 5). The seasonally averaged LST ranges from 294 K to 300 K in the Canadian boreal regions. Therefore, the reduction of canopy temperature in this region due to the

Table A1. Set of Equations for Each Component of Sensible (H), Latent (E), and CO_2 (A) Fluxes[a]

Sensible Heat Flux	Latent Heat Flux	CO_2 Flux
$H = -\rho_{atm} C_p \frac{(T_{atm} - T_{air})}{r_{ah}}$	$E = -\lambda \rho_{atm} \frac{(q_{atm} - q_{air})}{r_{aw}}$	$A = -\frac{(c_{atm} - c_{air})}{1.36 r_{aw}}$
$H_{sun} = -\rho_{atm} C_p (T_{air} - T_{sun}) \cdot \frac{f_{sun}(L+S)\cdot 2}{r_{b\_sun}}$	$E_{sun} = -\lambda \rho_{atm} \left(q_{air} - q_{sat}^{T_{sun}}\right) \cdot \left\{ \frac{f_{wet} f_{sun}(L+S)}{r_{b\_sun}} + \frac{f_{dry} f_{sun} L}{r_{b\_sun} + r_{s\_sun}} \right\}$	$A_{sun} = -\left(A_{leaf\_sun} - A_{d\_sun}\right) f_{sun} L$
$H_{sha} = -\rho_{atm} C_p (T_{air} - T_{sha}) \cdot \frac{f_{sha}(L+S)\cdot 2}{r_{b\_sha}}$	$E_{sha} = -\lambda \rho_{atm} \left(q_{air} - q_{sat}^{T_{sha}}\right) \cdot \left\{ \frac{f_{wet} f_{sha}(L+S)}{r_{b\_sha}} + \frac{f_{dry} f_{sha} L}{r_{b\_sha} + r_{s\_sha}} \right\}$	$A_{sha} = -\left(A_{leaf\_sha} - A_{d\_sha}\right) f_{sha} L$
$H_g = -\rho_{atm} C_p \frac{\left(T_{air} - T_g\right)}{r_{b\_soil}}$	$E_g = -\rho_{atm} \frac{\left(q_{air} - q_g\right)}{r_{b\_soil}}$	$A_g = A_{g\_ref} f(\Theta_g) f(T_g)$

[a] T represents temperature; q represents vapor mixing ratio; c represents CO_2 concentration; subscript *atm* represents the atmosphere 10 m above the canopy top; subscript *air* represents the air within the canopy space; subscript g represents the ground; ρ_{atm} is the dry air density at surface level; C_p is the specific heat of dry air at surface level; q_{sat} is saturated vapor mixing ration; f_{sun} and f_{sha} are sunlit and shaded fraction of vegetation; f_{wet} is wetted fraction of vegetation, and $f_{dry} = 1. - f_{wet}$; A_{l_sun} and A_{l_sha} are sunlit and shaded leaf photosynthesis; A_{d_sun} and A_{d_sha} are sunlit and shaded leaf dark (maintenance and growth) respiration; A_{g_ref} is reference soil respiration rate; r_{ah} and r_{aw} are dry air and moisture resistance between the canopy air and atmosphere 10 m above the canopy top height, which is derived from Monin-Obkhov similarity theory; r_{b_sun} and r_{b_sha} are resistance between sunlit, shaded leaves and canopy air, respectively; and r_{b_sun} is resistance between soil and canopy air.

aerosol light scattering effect lowers kinetic functions (f_T) and consequently the rubisco-limited photosynthesis rate.

[45] Overall, the aerosol light scattering effect becomes most productive for high-LAI and optimum temperature environments under cloudless-sky conditions around noon, and is least productive for low-LAI, low-temperature environments under cloud-sky conditions in early morning or late afternoon. As a result, domain-averaged plant productivity, measured as net primarily production, is changed by -0.71 g C m^{-2} (-0.09%) in 2000 and $+5.00$ g C m^{-2} ($+0.5\%$) in 2001. *Gu et al.* [2002], *Niyogi et al.* [2004], and *Chang* [2004] focused on their statistical sampling in cloudless sky from 1000 to 1400 local time, which corresponds to 1600 to 2000 UT in this domain. During this period, the aerosol light scattering effect becomes most positive. Thus, our results do not conflict with these previous studies. One noteworthy finding is that the aerosol light scattering effect seems to increase the amplitude of the daytime diurnal cycle of the carbon flux. This may have important implications for the carbon cycle science [e.g., *Denning et al.*, 1996].

[46] This study also examined the aerosol light scattering effect on the surface energy fluxes. The effect is unique in that aerosol loading alters the Bowen ratio by reducing sensible heat flux greater than latent heat flux especially over the forest regions (Figures 5 and 6). This result can be explained by a combination of (1) increased photosynthesis (stomatal conductance) and (2) decreased net surface radiation. First, as examined in section 3, the aerosol light scattering effect enhances diffuse radiation (Figure 3b) and shaded component canopy photosynthesis (Figure 7a), and consequently the net photosynthesis especially over the forests (Figure 5). This means that the stomatal resistance (r_s) is decreased (equation (1) in Table A2 in Appendix A). Second, the aerosol light scattering leads to a depression in net surface radiation and surface skin temperature (e.g., the fourth row of Figure 5 and Figure 6d). A slight reduction in canopy temperature (mainly represented by LST over the dense forest site), effectively lowers the saturated vapor mixing ratio (q_{sat}), because of the rapid transition of q_{sat} as a function of temperature. This eventually reduces the gradient between within-leaf saturated vapor mixing ratio (q_{sat}) and canopy air vapor mixing ratio (q_{air}). Thus, aerosol light scattering reduces r_s and ($q_{sat} - q_{air}$) that canceled out effects on latent heat flux in the equations of Table A1 in Appendix A. Depending on the degrees of reduction in each of r_s and ($q_{sat} - q_{air}$), sensitivity of latent heat flux can be varied in time and space. For example, forestlands tend to decrease r_s more than croplands in our simulation inferred from Figure 6a. With respect to the small (or no) reduction in latent heat flux, sensible heat flux must be reduced more in order to balance out the net reduction of surface energy budget due to the aerosol light scattering (equation (A1a, A1b) in Appendix A). This is why the spatial patterns in the lowest dH (dark purple regions) are consistent with the regions that have near-zero (white regions) dE, including the mixed and deciduous broadleaf forest in the southeastern United States and Canadian boreal region (the third row in Figure 5).

[47] These simulation results depend on the accuracy of the modeling framework in this study. Our modeling framework were rigorously tested and calibrated in the previous studies [*Matsui et al.*, 2004, 2007; *Matsui*, 2007], and shows good agreement with the measurements at the several Fluxnet sites in this study. There are still factors to be improved for future studies. These include the model treatment and understanding of (1) physiological characteristics in different croplands, (2) troposphere ozone effect (which often coincides with high aerosol loading) on the plant growth, (3) long-term behavior of plant carbon and nitrogen allocation for different light environments, (4) three-dimensional light scattering effect on canopy, and (5) land-atmosphere feedbacks, to name a few.

[48] In conclusion, all of these results suggest that the aerosol light scattering effect over land must be properly treated in climate models for better assessment of anthropogenic aerosol effects on climate and carbon cycles. For this, proper treatment of aerosol optical proprieties and light scattering in the radiative transfer model and sunlit-shaded multicanopy treatment are needed in the land surface model within the climate modeling framework.

Appendix A: Energy Budget and Photosynthesis Processes in Sun-Shade Scheme

[49] Energy budgets are diagnosed separately for sunlit and shaded canopy at every model time step. Canopy air is assumed to have zero heat capacity, i.e., net shortwave

Table A2. Set of Equations for the Empirical Stomatal Conductance and the Photosynthesis Model[a]

	Equation
(1)	$\frac{1}{r_s} = a\left(\frac{A_{leaf} e_{leaf} P_{atm}}{c_{leaf} e_i}\right) + b$
(2)	$A_{leaf} = \min\langle W_V, W_J, W_E\rangle$
(3)	$W_V = \begin{cases} V_m\left\{\frac{c_{leaf}-\Gamma^*}{c_{leaf}+k_c\left(1+o_{leaf}/k_o\right)}\right\}, & for\ C_3 \\ V_m, & for\ C_4 \end{cases}$
(4)	$W_J = \begin{cases} q_e\phi_{PAR}\left\{\frac{c_{leaf}-\Gamma^*}{c_{leaf}-2\Gamma^*}\right\}, & for\ C_3 \\ q_e\phi_{PAR}, & for\ C_4 \end{cases}$
(5)	$W_E = \begin{cases} 0.5V_m, & for\ C_3 \\ 20000V_m c_{leaf}/p, & for\ C_4 \end{cases}$
(6)	$A_d = \begin{cases} 0.015V_m, & for\ C_3 \\ 0.025V_m, & for\ C_4 \end{cases}$

[a]Stomatal conductance is represented by $1/r_s$, where r_s is stomatal resistance. T represents temperature, q represents vapor mixing ratio, e represents partial pressure of water vapor, c represents CO_2 concentration, O presents O_2 concentration, subscript *leaf* represents the leaf-level process, subscript *atm* represents the atmosphere 10 m above the canopy top, subscript *air* represents the air within the canopy space, Γ^* is CO_2 compensation point, k_c is the rubisco Michaels-Menten constant for CO_2, k_c is the rubisco inhibition constant for oxygen, q_e is the quantum yield of electron transport that depends on the land cover class, ϕ_{PAR} is absorbed PAR derived for unit sunlit and shaded LAI, and V_m is temperature- and water-limited maximum rate of rubisco-limited assimilation rate. Note that the stomatal conductance is separately derived for sunlit and shaded leaf; thus, e_{leaf}, V_m, and ϕ_{PAR} are also separately derived for sunlit and shaded components.

radiation (*SW*) equal to the sum of the net longwave radiation (*LW*), turbulent sensible (*H*) and latent heat (*E*) fluxes.

$$R_{sun} = SW_{sun} - LW_{sun} - H_{sun} - E_{sun} = 0 \qquad \text{(A1a)}$$

$$R_{sha} = SW_{sha} - LW_{sha} - H_{sha} - E_{sha} = 0 \qquad \text{(A1b)}$$

where subscript *sun* and *sha* represent the sunlit and shaded canopy, respectively. Both equations are solved with respect to the change in the sunlit and shaded vegetation temperature (T_{sun} and T_{sha}) via the Newton-Raphson iteration method [*Dai et al.*, 2004]. A complete description of each term is described in Table A1.

[50] Net solar radiation is separated into direct and diffuse radiation via an empirical relationship (see Appendix B). Net solar radiation and photosynthetically active radiation (PAR) on the canopy are computed by the modified two-stream canopy radiative transfer (TCRT) scheme [*Sellers*, 1985; *Matsui et al.*, 2007]. Sunlit vegetation receives both direct and diffuse radiation, while shaded vegetation receives only diffuse radiation [*Norman*, 1979]. The net absorbed PAR is computed in a similar manner by using visible band radiation only. The sunlit fraction of canopy (f_{sun}) is derived by the integration of within-canopy extinction coefficient (k_b) of sunfleck penetration over total leaf (L) and stem (S) area index [*Norman*, 1979]. The sunlit fraction of canopy associated with k_b is derived from the TCRT for every model time step during the daytime.

[51] Sunlit and shaded canopy stomatal conductance are coupled with the photosynthesis rate based on the semiempirical formulations by *Ball et al.* [1987] and *Collatz et al.* [1991] (Table A2). The carbon assimilation rate is the minimum among rubisco-limited rate (W_V), light-limited assimilation rate (W_J), and the carbon compound export limitation (W_E).

[52] In general, W_J is particularly important for shaded leaf photosynthesis, since it is generally a light-limited environment (i.e., $A_{l\_sha} = W_j$). W_J linearly depends on the quantum yield of electron transport ($q_e = 0.04$) (Table A2). W_V is particularly important for sunlit leaf photosynthesis since it is generally a light-saturated rubisco-limited environment (i.e., $A_{l\_sun} = W_V$). W_V linearly depends on the sunlit and shaded components of rubisco-limited photosynthetic capacity (V_m^{sun} and V_m^{sha}) (Table A2), which are kinetic functions (f_T) of bulk sunlit or shaded canopy temperature (T_{sun} or T_{sha}) and also a function of water stress ($f\Psi$), and scaled sunlit or shaded vegetation reference photosynthetic capacity (V_{ref}^{sun} or V_{ref}^{sha}).

$$V_m^{sun} = V_{ref}^{sun} f_{T_{sun}} f_\Psi \qquad \text{(A2a)}$$

$$V_m^{sha} = V_{ref}^{sha} f_{T_{sha}} f_\Psi \qquad \text{(A2b)}$$

The kinetic function is the combination of the Q_{10} function for the reference temperature (25°C) and the thermal breakdown of metabolic processes.

$$f_{T_{sun}} = \frac{a_{Q10}^{(T_{sun}-298.16)/10}}{1+\exp\left[(0.02a_{Q10}+0.1)(T_{sun}-T_{opt})\right]} \qquad \text{(A3)}$$

where a_{Q10} controls the shape of temperature function (Table A3); T_{opt} is an optimum temperature. The same function is applied for the shaded component, using shaded canopy temperature (T_{sha}). Higher (lower) a_{Q10} tends to generate a sharp (moderate) rise in temperature function and resultant photosynthesis capacity.

[53] V_{ref}^{sun} and V_{ref}^{sha} are analytically scaled from the canopy top photosynthesis capacity (V_{ref}^{top}) and within-canopy verti-

Table A3. Set of Tuning Parameters Defined in CSU ULM as Used in This Paper

Land Cover-Dependent Parameters	V_{ref}^{top}(μmol m^{-2} s^{-1})	a_n (−)	a_{Q10} (−)	q_e (−)
Evergreen needleleaf forests	38.3	0.5	2.9	0.04
Deciduous broadleaf forests	19.0	0.1	4.5	0.04
Mixed forests	17.6	0.1	7.0	0.04
Grasslands	10.8	0.5	2.8	0.04
Croplands	24.6	0.5	8.4	0.04

cal profile of sunfleck penetration and photosynthesis capacity for every model time step [*de Pury and Farquhar*, 1997].

$$V_{ref}^{sun} = \frac{\int_0^L V_{ref}^{top} e^{-k_n x} e^{-kx} dx}{\int_0^L e^{-kx} dx} \tag{A4a}$$

$$V_{ref}^{sha} = \frac{\int_0^L V_{ref}^{top} e^{-k_n x} (1 - e^{-kx}) dx}{\int_0^L (1 - e^{-kx}) dx} \tag{A4b}$$

where x is cumulative leaf area index, k_n is a within-canopy extinction coefficient of V_{ref}. (= $V_{ref}^{top}\ e^{-k_n x}$). k_n is usually related to the extinction of diffuse light for the total canopy and tuning parameter.

$$k_n = a_n k_d, \tag{A5}$$

where k_d is the within-canopy diffuse light extinction, and a_n is a tuning parameter (Table A3).

Appendix B: Estimation of Diffuse Radiation From Global Irradiance From ISIS Observations

[54] A sun-shade canopy scheme requires the proper separation of solar radiation into diffuse and beam components [*Gu et al.*, 2002]. The diffuse radiation fraction, DRF (R_d/R_g, where R_d is diffuse solar irradiance and R_g is total global irradiance at the surface), is often estimated from the transmittance (R_g/R_{ext}, where R_{ext} is extraterrestrial global irradiance). *Roderick* [1999] used a stepwise linear function to fit the DRF and transmission with daily and monthly averaged insolation data. This study used the Integrated Surface Irradiance Study (ISIS): NOAA surface-based solar monitoring programs, which provides instantaneous surface radiation data, including direct and diffuse at broadband and PAR band with consistency and accuracy based on reference standards maintained at levels better than 1% at nine different sites in the United States [*Hicks et al.*, 1996]. Nine ISIS sites are chosen from the conterminous United States.

[55] A total of 42,961 instantaneous radiation observations and binned averaged values from every site are compiled in the scatterplots as a function of cosine of solar zenith angle (u) (Figure B1). Patterns of averaged DRF values appear to be close to the stepwise function given by *Roderick* [1999]. Unlike the linear stepwise function, the derived value shows a slight decrease in DRF for $0.05 \sim 0.3$ of transmittance. The lowest peak of DRF is at 0.8 of transmittance, which is consistent with the results given by *Roderick* [1999]. For high u, DRF are constantly high for the low-transmittance range ($\sim$0.3), and DRF decrease rapidly for higher transmittance (0.4$\sim$0.8, and becomes the lowest DRF for 0.85 of transmittance. As the u_0 decrease, the lowest DRF values slightly increase, being highest for u = 0.05. This unique solar angle dependence could explain the slight difference of the DRF transmittance relationship in different studies discussed by *Roderick* [1999]: that is, latitudinal difference and u_0 tendencies between the sites results in slightly different DRF transmission relationships.

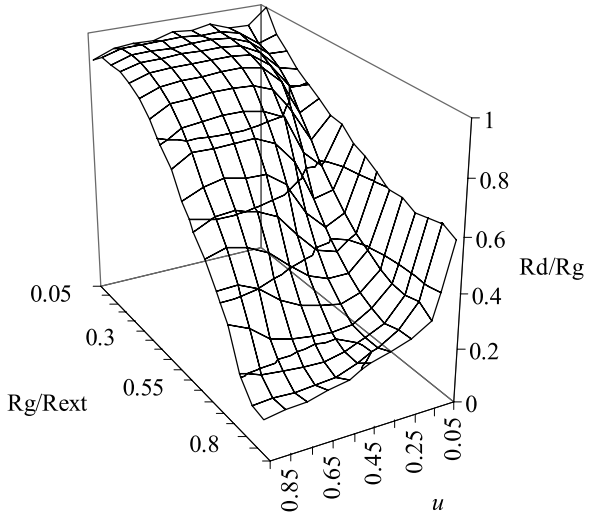

Figure B1. Diffuse radiation fraction (Rd/Rg) as a function of transmittance (Rg/Rext) and cosine of solar zenith angle (u).

[56] In practice, the values in Figure B1 are utilized as a look-up table, to separate NLDAS shortwave radiation into the diffuse and beam radiation as a function of transmittance and solar zenith angle.

Appendix C: A Simple Retrieval of Cloud Optical Depth From the GOES-Derived Surface Downwelling Shortwave Radiation

[57] Appendix C explains a simple retrieval of cloud optical depth (COD) and cloud liquid water path (CLWP) from the NLDAS surface downwelling shortwave radiation (SW). The goal of the algorithm is to derive the cloud properties that reproduce the realistic all-sky (clear + cloudy) downwelling shortwave radiation with and without aerosol loading through a radiative transfer code.

[58] This simple retrieval uses the NASA Langley version of the Fu-Liou code (NFL) [*Fu and Liou*, 1993; *Charlock et al.*, 2004]. The vertical profile of atmospheric temperature, water vapor mixing ratio, and ozone mixing ratio are derived from a midlatitude summer climatological sounding [*McClatchey et al.*, 1972]. Surface broadband albedo is set to 0.1.

[59] A relationship between top-of-atmosphere (TOA: S_{TOA}) and surface downwelling shortwave radiation in clear sky (SW_{clear}) is given by the simple Beer's law

$$SW_{clear} = SW_{TOA} e^{-k_{clear}/u} \tag{C1}$$

where k_{clear} is the extinction coefficient of clear sky (absorption and Rayleigh scattering of molecular), and u is the cosine of the solar zenith angle. For a given

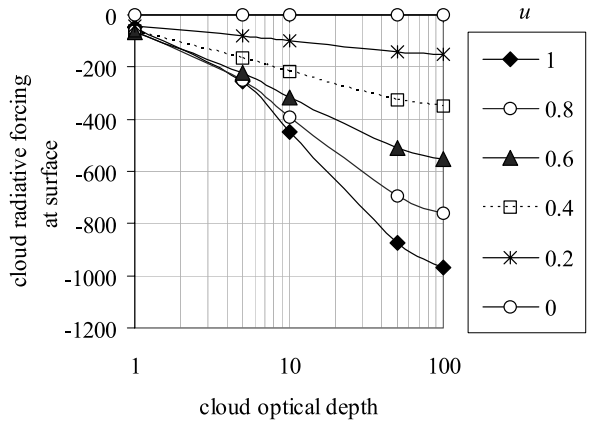

Figure C1. Variation of ΔSW (cloud radiative forcing at the surface on the y axis) (W m^{-2}) as functions of the cosine of the solar zenith angle (u) and cloud optical depth (COD).

climatological vertical profile and surface albedo, the variation of k_{clear} (therefore SW_{clear}) is explained by the fourth-order polynomial fit as a function of u, using the NFL code.

$$k_{clear} = -0.728u^4 + 1.795u^3 - 1.597u^2 + 0.775u + 0.003 \quad \text{(C2)}$$

[60] The shortwave cloud radiative forcing is defined as

$$\Delta SW = SW_{cloudy} - SW_{clear} \quad \text{(C3)}$$

where SW_{cloudy} is cloudy-sky surface downwelling shortwave radiation. ΔSW is also a function of cloud properties if SW_{clear} is known as a priori. Because of the one broadband of NLDAS SW, cloud properties are constrained as follows: (1) cloud is in liquid phase (not ice phase), (2) cloud is distributed from 600 mbar to 800 mbar, (3) cloud fraction is unity, and (4) cloud effective radius is 8 μm (assuming continental cloud). For a given constrains, a relationship between ΔSW and cloud optical depth (COD) is derived for different u via NFL code (Figure C1).

[61] For a given relationship in Figure C1, COD is inversely derived for a given u and NLDAS SW: (1) derive the difference between NLDAS SW and estimated SW_{clear} (using the equation (C3)) for a given u by using the relationship in equation (C2) and (2) if ΔSW is greater than ΔSW of COD = 1, COD is estimated by the relationship in Figure C1.

[62] In this retrieval, ΔSW less than that of COD = 1 is not considered as cloud. Because NLDAS SW was derived with the specific assumptions of aerosol climatology and vertical profile of temperature, humidity, and ozone [*Pinker et al.*, 2003], ΔSW in these low ranges can be the radiative forcing background aerosols or uncertainties of using sounding climatology in the algorithm ($\sim$10% of error). According to the probability density function of aerosol optical depth (AOD) over the eastern United States [*Matsui et al.*, 2004], 99.5% is distributed below an AOD of 0.65. For the radiative forcing of AOD of 0.65 (sulfate), ΔSW is less (67$\sim$84%) than ΔSW for COD = 1.

[63] Finally CLWP is derived from the assumed cloud droplet effective radius (R_e = 8μm) and the derived COD via

$$CLWP = \frac{\rho_w \cdot COD \cdot R_e}{1.5} \quad \text{(C4)}$$

[64] **Acknowledgments.** This work is funded by NASA CEAS fellowship (NAG512105), NASA Radiation (NNG04GB87G, NNX07AG35G_S01), and NASA Interdisciplinary Sciences (NNG04GL61G, NNX06AG74G_S02). The authors thank Brian Cosgrove and Kristi Arsenault for providing the NLDAS forcing data set and Jim Geiger and Sujay Kumar for developing/installing the NASA Land Information System. The authors also thank Hal Maring at NASA HQ for providing additional funding to cover the publication cost.

References

Baldocchi, D. D., et al. (2001), FLUXNET: A new tool to study the temporal and spatial variability of ecosystem-scale carbon dioxide, water vapor and energy flux densities, *Bull. Am. Meteorol. Soc.*, *82*, 2415–2434, doi:10.1175/1520-0477(2001)082<2415:FANTTS>2.3.CO;2.

Ball, I., E. Woodrow, and J. A. Berry (1987), A model predicting stomatal conductance and its contribution to the control of photosynthesis under different environmental conditions, in *Progress in Photosynthesis Research*, vol. 1, edited by J. Biggins, pp. 221–234, Martinus Nijhoff, Dordrecht, Netherlands.

Chameides, W. L., et al. (1999), Case study of the effects of atmospheric aerosols and regional haze on agriculture: An opportunity to enhance crop yields in China through emission controls?, *Proc. Natl. Acad. Sci. U. S. A.*, *96*, 13,626–13,633, doi:10.1073/pnas.96.24.13626.

Chang, H. (2004), Direct observations of aerosol effects on carbon and latent heat fluxes, M. S. thesis, Dep. of Mar., Earth, and Atmos. Sci., N. C. State Univ., Raleigh. (Available at http://landsurface.org)

Charlock, T. P., F. G. Rose, D. A. Rutan, D. Fillmore, and W. Collins (2004), All-sky aerosol direct forcing to SW and LW at TOA and surface using CERES Terra and the MATCH assimilation, paper presented at International Radiation Symposium, Int. Radiat. Comm., Int. Assoc. of Meteorol. and Atmos. Sci., Busan, South Korea, 23–28 Aug.

Chin, M., D. A. Chu, R. Levy, L. A. Remer, Y. J. Kaufman, B. N. Holben, T. Eck, and P. Ginoux (2004), Aerosol distribution in the northern hemisphere during ACE-Asia: Results from global model, satellite observations, and Sun photometer measurements, *J. Geophys. Res.*, *109*, D23S90, doi:10.1029/2004JD004829.

Cohan, D. S., J. Xu, R. Greenwald, M. H. Bergin, and W. L. Chameides (2002), Impact of atmospheric aerosol light scattering and absorption on terrestrial net primary productivity, *Global Biogeochem. Cycles*, *16*(4), 1090, doi:10.1029/2001GB001441.

Collatz, G. J., J. T. Ball, C. Grivet, and J. A. Berry (1991), Physiological and environmental regulation of stomatal conductance, photosynthesis and transpiration: A model that includes a laminar boundary layer, *Agric. For. Meteorol.*, *54*, 107–136, doi:10.1016/0168-1923(91)90002-8.

Cosgrove, B. A., et al. (2003), Real-time and retrospective forcing in the North American Land Data Assimilation System (NLDAS) project, *J. Geophys. Res.*, *108*(D22), 8842, doi:10.1029/2002JD003118.

Dai, Y., R. E. Dickinson, and Y.-P. Wang (2004), A two-big-leaf model for canopy temperature, photosynthesis, and stomatal conductance, *J. Clim.*, *17*, 2281–2299, doi:10.1175/1520-0442(2004)017<2281:ATMFCT>2.0.CO;2.

Denning, A. S., D. A. Randall, G. J. Collatz, and P. J. Sellers (1996), Simulations of terrestrial carbon metabolism and atmospheric CO_2 in a general circulation model. Part 2: Spatial and temporal variations of atmospheric CO_2, *Tellus, Ser. B*, *48*, 543–567.

de Pury, D. G. G., and G. D. Farquhar (1997), Simple scaling of photosynthesis from leaves to canopies without the errors of big-leaf models, *Plant Cell Environ.*, *20*, 537–557, doi:10.1111/j.1365-3040.1997.00094.x.

Fu, Q., and K.-N. Liou (1993), Parameterization of the radiative properties of cirrus clouds, *J. Atmos. Sci.*, *50*, 2008–2025, doi:10.1175/1520-0469(1993)050<2008:POTRPO>2.0.CO;2.

Goudriaan, J. (1977), *Crop Micrometeorology: A Simulation Study*, 249 pp., Cent. for Agric. Publ. and Doc., Wageningen, Netherlands.

Gu, L., D. Baldocchi, S. B. Verma, T. A. Black, T. Vesala, E. M. Falge, and P. R. Dowty (2002), Advantages of diffuse radiation for terrestrial ecosystem productivity, *J. Geophys. Res.*, *107*(D6), 4050, doi:10.1029/2001JD001242.

Gu, L., D. D. Baldocchi, S. C. Wofsy, J. W. Munger, J. J. Michalsky, S. P. Urbanski, and T. A. Boden (2003), Response of a deciduous forest to the

Mount Pinatubo eruption: Enhanced photosynthesis, *Science*, *299*, 2035–2038, doi:10.1126/science.1078366.

Hansen, M. C., R. S. Defries, J. R. G. Townshend, and R. Sohlberg (2000), Global land cover classification at 1km spatial resolution using a classification tree approach, *Int. J. Remote Sens.*, *21*, 1331–1364, doi:10.1080/014311600210209.

Hess, M., P. Koepke, and I. Schult (1998), Optical properties of aerosols and clouds: The software package OPAC, *Bull. Am. Meteorol. Soc.*, *79*, 831–844, doi:10.1175/1520-0477(1998)079<0831:OPOAAC>2.0.CO;2.

Hicks, B. B., J. J. DeLuisi, and D. R. Matt (1996), The NOAA integrated surface irradiance study (ISIS)—A new surface radiation monitoring program, *Bull. Am. Meteorol. Soc.*, *77*, 2857–2864, doi:10.1175/1520-0477(1996)077<2857:TNISIS>2.0.CO;2.

Kalnay, E., et al. (1996), The NCEP/NCAR 40-year reanalysis project, *Bull. Am. Meteorol. Soc.*, *77*, 437–471, doi:10.1175/1520-0477(1996)077<0437:TNYRP>2.0.CO;2.

Kanniah, K., N. Tapper, J. Beringer, X. Zhu, and C. Long (2006), Preliminary investigations of the role of smoke aerosols on carbon uptake of a northern Australian tropical savanna, paper presented at Atmospheric Radiation and Measurement Science Team Meeting, U.S. Dep. of Energy, Albuquerque, N. M., 27–31 March.

Krakauer, N. Y., and J. T. Randerson (2003), Do volcanic eruptions enhance or diminish net primary production? Evidence from tree rings, *Global Biogeochem. Cycles*, *17*(4), 1118, doi:10.1029/2003GB002076.

Kumar, S. V., et al. (2006), Land information system—An interoperable framework for high resolution land surface modeling, *Environ. Model. Softw.*, *21*, 1402–1415, doi:10.1016/j.envsoft.2005.07.004.

Law, B. E., et al. (2002), Environmental controls over carbon dioxide and water vapor exchange of terrestrial vegetation, *Agric. For. Meteorol.*, *113*, 97–120, doi:10.1016/S0168-1923(02)00104-1.

Lin, J. C., T. Matsui, R. A. Pielke Sr., and C. Kummerow (2006), Effects of biomass burning-derived aerosols on precipitation and clouds in the Amazon Basin: A satellite-based empirical study, *J. Geophys. Res.*, *111*, D19204, doi:10.1029/2005JD006884.

Malm, W. C., B. A. Schichtel, M. L. Pitchford, L. L. Ashbaugh, and R. A. Eldred (2004), Spatial and monthly trends in speciated fine particle concentration in the United States, *J. Geophys. Res.*, *109*, D03306, doi:10.1029/2003JD003739.

Matsui, T. (2007), Aerosol effects on cloud-precipitation and land-surface processes, Ph.D. dissertation, 262 pp., Dep. of Atmos. Sci., Colo. State Univ., Fort Collins.

Matsui, T., S. M. Kreidenweis, R. A. Pielke Sr., B. Schichtel, H. Yu, M. Chin, D. A. Chu, and D. Niyogi (2004), Regional comparison and assimilation of GOCART and MODIS aerosol optical depth across the eastern U.S., *Geophys. Res. Lett.*, *31*, L21101, doi:10.1029/2004GL021017.

Matsui, T., H. Masunaga, S. M. Kreidenweis, R. A. Pielke Sr., W.-K. Tao, M. Chin, and Y. Kaufman (2006), Satellite-based assessment of global warm cloud properties associated with aerosols, atmospheric stability, and diurnal cycle, *J. Geophys. Res.*, *111*, D17204, doi:10.1029/2005JD006097.

Matsui, T., A. Beltrán-Przekurat, R. A. Pielke Sr., D. Niyogi, and M. B. Coughenour (2007), Continental-scale multiobservation calibration and assessment of Colorado State University Unified Land Model by application of Moderate Resolution Imaging Spectroradiometer (MODIS) surface albedo, *J. Geophys. Res.*, *112*, G02028, doi:10.1029/2006JG000229.

McClatchey, R. A., W. Fenn, J. E. A. Selby, F. E. Volz, and J. S. Garing (1972), Optical properties of the atmosphere, *Environ. Res. Pap.*, 411, 108 pp., Air Force Cambridge Res. Lab., Hanscom Air Force Base, Mass.

Mera, R. J., D. Niyogi, G. S. Buol, G. G. Wilkerson, and F. Semazzi (2006), Potential individual versus simultaneous climate change effects on soybean (C3) and maize (C4) crops: An agrotechnology model based study, *Global Planet. Change*, *54*, 163–182, doi:10.1016/j.gloplacha.2005.11.003.

Miller, D. A., and R. A. White (1998), A conterminous United States multilayer soil characteristics data set for regional climate and hydrology modeling, *Earth Interact.*, *2*, 1–26, doi:10.1175/1087-3562(1998)002<0002:CUSMS>2.0.CO;2.

Min, Q. (2005), Impact of aerosols and clouds on forest-atmosphere carbon exchange, *J. Geophys. Res.*, *110*, D06203, doi:10.1029/2004JD004858.

Misson, L., M. Lunden, M. Mc Kay, and A. H. Goldstein (2005), Atmospheric aerosol light scattering and surface wetness influence the diurnal pattern of net ecosystem exchange in a semi-arid ponderosa pine plantation, *Agric. For. Meteorol.*, *129*, 69–83, doi:10.1016/j.agrformet.2004.11.008.

Myneni, R. B., et al. (2002), Global products of vegetation leaf area and fraction absorbed PAR from year one of MODIS data, *Remote Sens. Environ.*, *83*, 214–231, doi:10.1016/S0034-4257(02)00074-3.

Niyogi, D., et al. (2004), Direct observations of the effects of aerosol loading on the net ecosystem CO_2 exchanges over different landscapes, *Geophys. Res. Lett.*, *31*, L20506, doi:10.1029/2004GL020915.

Norman, J. M. (1979), Modeling the complete crop canopy, in *Modification of the Aerial Environment of Crops*, edited by B. J. Barfield and J. F. Gerber, pp. 249–280, Am. Soc. Agric. Eng., St. Joseph, Mich.

Oliveira, P. H. F., P. Artaxo, C. Pires, S. D. Lucca, A. Procopio, B. Holben, J. Schafer, L. F. Cardoso, S. C. Wofsy, and H. R. Rocha (2007), The effects of biomass burning aerosols and clouds on the CO_2 flux in Amazonia, *Tellus, Ser. B*, *59*(3), 338–349, doi:10.1111/j.1600-0889.2007.00270.x.

Pinker, R. T., et al. (2003), Surface radiation budgets in support of the GEWEX Continental-Scale International Project (GCIP) and the GEWEX Americas Prediction Project (GAPP), including the North American Land Data Assimilation System (NLDAS) project, *J. Geophys. Res.*, *108*(D22), 8844, doi:10.1029/2002JD003301.

Rocha, A. V., H. B. Su, C. Vogel, H. P. Schmid, and P. S. Curtis (2004), Photosynthetic and water use efficiency responses to diffuse radiation by an aspen-dominated northern hardwood forest, *For. Sci. Washington D. C.*, *50*, 793–801.

Roderick, M. L. (1999), Estimating the diffuse component from daily and monthly measurements of global radiation, *Agric. For. Meteorol.*, *95*, 169–185, doi:10.1016/S0168-1923(99)00028-3.

Roderick, M. L., G. D. Farquhar, S. L. Berry, and I. R. Noble (2001), On the direct effect of clouds and atmospheric particles on the productivity and structure of vegetation, *Oecologia*, *129*, 21–30, doi:10.1007/s004420100760.

Rossow, W. B., and R. A. Schiffer (1991), ISCCP cloud data products, *Bull. Am. Meteorol. Soc.*, *72*, 2–20, doi:10.1175/1520-0477(1991)072<0002:ICDP>2.0.CO;2.

Sellers, P. J. (1985), Canopy reflectance, photosynthesis and transpiration, *Int. J. Remote Sens.*, *6*, 1335–1372, doi:10.1080/01431168508948283.

Spinhirne, J. D., J. A. Reagan, and B. M. Herman (1980), Vertical distribution of aerosol extinction cross section and inference of aerosol imaginary index in the troposphere by lidar technique, *J. Appl. Meteorol.*, *19*, 426–438, doi:10.1175/1520-0450(1980)019<0426:VDOAEC>2.0.CO;2.

Tao, W.-K., X. Li, A. Khain, T. Matsui, S. Lang, and J. Simpson (2007), Role of atmospheric aerosol concentration on deep convective precipitation: Cloud-resolving model simulations, *J. Geophys. Res.*, *112*, D24S18, doi:10.1029/2007JD008728.

Wang, Y.-P., and R. Leuning (1998), A two-leaf model for canopy conductance, photosynthesis and partitioning of available energy. I. Model description and comparison with a multilayered model, *Agric. For. Meteorol.*, *91*, 89–111, doi:10.1016/S0168-1923(98)00061-6.

A. Beltrán-Przekurat and R. A. Pielke Sr., Department of Atmospheric and Oceanic Sciences, Cooperative Institute for Research in Environmental Sciences, University of Colorado, Boulder, CO 80309, USA.

M. Coughenour, Natural Resource and Environmental Laboratory, Colorado State University, Fort Collins, CO 80523, USA.

T. Matsui, NASA Goddard Space Flight Center, Code 613.1, Greenbelt, MD 20771, USA. (matsui@agnes.gsfc.nasa.gov)

D. Niyogi, Department of Agronomy, Purdue University, West Lafayette, IN 47906, USA.